A review for J. Electrochem. Soc. *Accepted April 27, 2022*

Review - Carbon Cloth as a Versatile Electrode: Manufacture, Properties, Reaction Environment and Applications

María I. León [1], Locksley F. Castañeda [2], Ana A. Márquez [1],

Frank C. Walsh [3], José L. Nava [1, z]

[1] *Department of Geomatic and Hydraulic Engineering, University of Guanajuato, Av. Juárez 77, Centro, 36000, Guanajuato, Guanajuato, Mexico.*

[2] *CONACYT – Department of Geomatic and Hydraulic Engineering, University of Guanajuato, Av. Juárez 77, Centro, 36000, Guanajuato, Mexico.*

[3] *Electrochemical Engineering Laboratory, Energy Technology Research Group, Engineering Sciences, University of Southampton, Highfield, Southampton, SO17 1BJ, United Kingdom.*

Email:	(María I. León)	mi.leonsotelo@ugto.mx
	(Locksley F. Castañeda)	lfcu@ugto.mx
	(Ana A. Márquez)	aa.marquezvargas@ugto.mx
	(Frank C. Walsh)	F.C.Walsh@soton.ac.uk
	[z](José L. Nava)	jlnm@ugto.mx

(Approx. 14 000 words, 18 reactions/equations, 3 tables, 11 figures and 200 references).

Abstract

The manufacture, characterisation and application of carbon cloth (CC) are reviewed and its use as an electrode in fundamental electrochemical studies and technological applications over the last fifty-five years is considered. The most widely used precursors to produce commercial CC are polyacrylonitrile (PAN) fibres manufactured by heat treatment at 1500-3000 ^{o}C. Carbon cloth has good electrical conductivity, high mechanical strength and high chemical resistance. CC is a versatile electrode material that can operate over a wide potential range in aqueous electrolytes and molten salts. Chemical and thermal methods can enhance the surface area and help to control the wettability of CC surfaces. Electrodes can be decorated by nanostructured carbons, precious metal nanoparticles or enzyme immobilisation to modify surface functionality, improve activity and widen applications. The doping of CC with polymers, metals and metal oxides has enabled its use in sensors, electrosynthesis of chemicals, environmental remediation and water treatment as well as energy storage and conversion. Electrochemical cells incorporating CC, which range from three-electrode laboratory bench cells to pilot plant flow cells, are illustrated. The characterisation of hydrodynamics, mass transport rates and potential/current distributions in CC-equipped flow cells, using experimental and computational fluid dynamics approaches, are analysed. Finally, continuing research challenges to CC are highlighted.

Keywords: Weave pattern, structural properties, mass transport, surface area.

Contents

Energy storage and conversion

Static batteries

Redox flow batteries

Supercapacitors

Fuel cells

Microbial fuel cells

Summary

Recommendations for further research and development

Introduction

The present work reviews the main features of CC as an electrode in electrochemistry Applications in sensing and monitoring, kinetics, synthesis, environmental remediation and water treatment, energy storage and conversion are considered. The advantages provided by CC are explained in terms of its structure and physicochemical properties. The benefits of CC are highlighted. The most widely exploited feature of the CC electrode is the large surface area offered after cloth treatment,[1] often by functionalisation with heteroatoms,[2-4] metals,[5] hydro/oxides,[6-7] nanoparticulate carbon materials,[8] or miscellaneous dopants. The advantage of CC surface treatment over other carbonaceous materials, such as carbon paper, lies in a woven bundle of carbon filaments, allowing the exclusion of binders needed to manufacture carbon paper (CP) electrodes. The binders partially disable valuable surface area for electrochemical reactions.[8] Other important CC characteristics are based on the high permeability provided by the large porosity and low tortuosity which enhance mass, ion and electron transport properties.[9-11] Despite such benefits, the structure of CC electrodes, such as the cloth weaving/knitting pattern, thickness of the cloth yarns (i.e., the number of filaments) and the cloth tightening, are not widely appreciated. The possible impact of specific cloth patterns or designs on the electrochemical systems might enhance the system's performance. Once the cloth pattern is chosen, a higher filament count, surface area for specific end functionalisation are important characteristics. In addition, tightening of yarns contributes to the available surface area. From these structural features, the behaviour of flow systems incorporating CC electrodes are relevant to cell design and electrochemical processing. In this respect, there are unanswered questions about woven CC since few studies focus on structural characteristics and the way in which they determine electrochemical performance. Readers are encouraged to explore relationships between structure, properties,

and electrochemical behaviour of CC electrodes to improve cell modelling and optimization. The following sections discuss the manufacture of CC along with its structure and properties, highlighting the features and potential study areas for possible improvements in electrochemical performance. The cell design, reaction environment and electrode performance of reactors incorporating CC electrodes are analysed. When considering the versatility offered by a CC electrode in terms of its shape, lightweight nature, low thicknesses and reproducibility,[2] some actual example applications are provided, from laboratory to industrial scale. CC electrode trends and suggestions for further research are provided.

Manufacture, structure and properties

CC contains at least 92-99% by weight carbon, which may include graphite.[12] The structural base of CC is a woven bundle of carbon fibres (yarns), which provide the material with high electrical and thermal conductivity, high mechanical strength, high thermal and chemical stability and low density. CC electrodes are widely employed in electrochemical processes, commonly as catalyst supports. In the mid-1960s, the use of CC as an auxiliary electrode in nickel/cadmium cells[13] was explored; its applications continued to widen in the years ahead, CC electrodes being used in sensing/monitoring, electrode kinetics, electrosynthesis and processing, environment remediation, energy storage and energy conversion, among others (Fig. 1).

The oldest known work related to electrode CC, due to Grieger (1965)[13] is based on the description of properties seen in early fuel cell research and a platinized CC auxiliary electrode in primary batteries. The following is a concise description of CC properties given by Grieger: it is unbreakable, can be cut into any shape, tightly folded and rolled for easy

incorporation in cells, its lightweight nature (≈ 3×10^{-2} g cm^{-2}) and low thickness add negligible weight and volume in compressed systems, it does not require waterproofing and easy to replicate. The surface of CC can be modified by electrodeposition and presents good reproducibility at temperatures from 25 to -40 °C. After soaking in KOH (30%), CC catalyses H_2 and O_2 evolution, is relatively cheap and electrical connections are readily made by light compression against a metallic current collector.[13]

Manufacture

In practice, carbon fibre (CF) is the CC base material. CF is usually obtained from carbon-rich precursors, such as pitch (coal- or petroleum-based) and polyacrylonitrile, PAN (acrylic-based), the most common precursors for CC electrodes. Depending on the precursor type, the properties of the fibres will differ significantly from each other, despite the essential processes for CF production being similar.[14-15] Carbon fibre production can proceed via three stages: stabilisation, carbonisation and graphitisation, as shown in Fig. 2A. The first stage is controlled oxidation (200-300 °C) in an air atmosphere to form a physically stable fibre by promoting the crosslinking of the precursor. Once the fibres have stabilised, those are carbonised (1500-2000 °C) in an inert atmosphere resulting in a turbostratic carbon phase aligned along the filament. The graphitisation (2000-3000 °C) cures the turbostratic defects providing a better alignment between layers. A higher carbon concentration is achieved in this stage.[16] It is important to mention that rayon (cellulose-based) and cotton precursors are also used to obtain activated carbon fibres (ACF), in which an activation step (700-1000 °C) is introduced instead of the graphitization step.[17] The resulting material properties of rayon fibres ACF differ significantly from the pitch and PAN fibres CF. For example, the specific surface area (BET surface) of ACF is up to 700 m^2 g^{-1}, while for CF is less than 1 m^2 g^{-1}.[18]

An analysis of material and energy requirements for the production of carbon felts from PAN and rayon was presented by Minke and coworkers (2017).[19] They demonstrated that despite the differences in the carbonization yield, ≈50% for PAN and ≈25% for rayon, the total energy consumption is similar each other, near 600 MJ (g carbon felt K)$^{-1}$, but regarding the global warming potential felts produced from PAN generates even to 18 kg CO_2 (kg carbon felt)$^{-1}$ *vs* 1.2 kg CO_2 (kg carbon felt)$^{-1}$ generated by rayon felt. In the cost assessment, until 2017, the manufacturing costs of one kg of PAN carbon felt was about 40 euros, while for the rayon carbon felt, the price rose to 65 euros.[19] It is important to carry out a detailed and in-depth analysis of manufacturing techniques and costs, aligned to environmental impact, in view of the rising demand on carbonaceous electrodes based on fibres. In this review, we focus on the structure and characteristics of CC which enable diverse applications in electrochemistry.

Regarding mechanical properties, a higher alignment of carbon layers will lead to a greater fibre tensile modulus, following the classification for fibre precursors of ultra-high modulus (> 500 GPa), high modulus (> 300 GPa), intermediate modulus (> 200 GPa), low modulus (100 < GPa) and high resistance (> 4 GPa).[20] For the cellulose-fibre precursor, a low tensile strength (1 GPa) has been identified.[21] There is no exclusive application of specific precursors to produce ACF or CF and a more detailed description of the carbon fibre manufacturing process can be found elsewhere.[14-18,20-21]

Regarding the production of CC, textile cloth can be used directly as a precursor. Typically, CC manufacturing requires cloth production followed by stabilisation, carbonisation and graphitisation stages. As shown in Fig. 2B, cloth production starts with fibres spinning, where the precursor polymers are converted into continuous fibres. Subsequently, a bundle of

filaments is gathered together and twisted during the yarn spinning. The yarns are weaved or knitted to obtain the cloth in the finishing process.[21] Patent reports propose the CC production by oxidising polymer fibres before weaving to provide cloth of oxidised yarns, then carbonise the latter to provide CC.[22-23] There are some other processes for CF handling, which involve the use of fibre staples instead of continuous fibre, to create felts or papers.[21] However, the latter is outside the scope of this review.

The woven cloth construction is made by interlacing two sets of yarns, the longitudinal (warp) and the transverse (weft) yarn; interlocking loops between yarns form the knitted cloth. The variation of interlocking or interlacing allows different cloth designs, for example, plain, twill and satin, Fig. 2C.[21,24] As discussed later in the "Properties" section, these design variations result in different cloth properties relating the permeability, porosity, and the above mentioned mechanical properties.[25-26] The resulting cloths have different properties to single carbon fibres regarding specific area and strength/tensile modulus.[27]

Structure

Since the CC is made of CF, there are two different ways to observe the structure of the CC. First, suppose one goes to the CC depths until reaching each fibre surface. Several carbon atom layers are arranged in regular patterns, be they graphitic, turbostratic or hybrid, depending on the precursors and the manufacturing processes. Although there is a distinction in manufacturing temperature interval for CF to obtain graphite fibres (graphitisation) or carbon fibres (carbonisation), not all precursors allow the complete formation of graphite structures.[28] The spacing between the layers is approx. 0.3375 nm, depending on whether the CF region is graphitic (0.335 nm) or turbostratic (0.34 nm). A stack of carbon layers forms a

basic structural unit (BSU), and a group of BSU together forms a microdomain. The collection of microdomains represents the fine structure of the CF. It is important to highlight that the microdomains are interspersed with pores formed during the elimination of heteroatoms from the precursor fibre in the production stages.[21] Second, the cloth design provides different geometrical structures that can be better appreciated when taking a cloth section in the longitudinal or transverse directions (for weaved cloths). The length and diameter of the longitudinal yarn, the deflected amount from a straight line, and the distance between the transverse yarns are related [29] (Fig. 2D). Similarly, there should be a relationship to the transverse yarn. Additional to these relations, the character of cloth is determined by the thread per inch, count of yarns and twist of yarns, and can be defined by the total number of weft and warp yarns in unit area (traditionally one square inch) of cloth, the yarn thickness, and the turns around the axis of one inch of yarn, respectively. In addition, the weaving type and setting conditions, the tension of the yarns, and the finishing treatments provide a large number of mechanical, thermal and permeable properties to the cloth, among others.[30] Thus, the description of each cloth type structure would lead us to a different topic than this work. Most of the reported works using a CC electrode associate the properties of the electrode to their system performance and electrode surface area, and not directly to each cloth type structure. This review focuses on the properties of the basic structures (plain, twill and satin) unless otherwise mentioned.

Structural Properties

As previously mentioned, the characteristics of CC are closely related to the carbon fibre base-precursor and its manufacturing process. As an electrode, the most attractive characteristics for CC are its low electrical resistivity, chemical and thermal stability,

biocompatibility, high mechanical strength, surface porosity, and wide potential window for the oxidation and reduction of an aqueous supporting electrolyte.[20,31] The woven structures are provided with high strength and stability in the manufacturing process, compared with drapeability and extensibility of knitted cloth . In terms of weave types in Fig. 2C, the plain pattern provides many yarns intersections, mutually binding themselves to give a stiffer cloth. The twill pattern provides half or fewer yarns intersection than the plain pattern, making this design a much flexible material. In the case of satin patterns, one longitudinal yarn is put over several transverse yarns, resulting in "unbalanced" yarn layers, in which most of the longitudinal reinforcement is in the top surface, while most transverse reinforcement is in the bottom surface. These reinforcements provide the cloth with a more flexible capability in one direction with respect to the other. The knitted fabrics easily distortions due to their looped structure. In addition to the ease of handling the cloth given by the weave patterns, it is crucial to consider the range of area per unit weight for each cloth and the number of filaments in the yarns since those directly impact the thickness of the cloth.[32] In Table 1, several cloth types and structural properties are listed. It can be seen that, for a given weave type and filament count, different area per unit weight is obtained. By comparing plain HF84 and HF130 cloths with the same filament count, it is possible to detect a difference in the weight per unit area, values of 84 and 127 g m^{-2}, respectively being found. Tightening of the yarns can explain this; higher values suggest a more tightened cloth. Since most CC electrode applications are focused on t high surface area, this feature can further benefit the electrochemical cell design if the cloth pattern is customised if modern weaving devices are considered. In accordance with A. A. Wong *et al.* (2020), the custom patterns could be tailored with a preferential response to desired properties, such as the direction of fluid flow,[9] as discussed in the redox flow battery section. Since most CC electrode applications are

focused on a high surface area, this feature can benefit electrochemical reactor design without sacrificing the benefits offered by available cloth patterns.

The different cloth fibre arrangement creates high porosity ($\varepsilon > 0.6$), a wide range of pore geometries and pore size distribution, low tortuosity, cloth density, and net-shape capabilities.[10] The cloth pores are conformed by void spaces between the yarns' overlap sections, the fibre-to-fibre distance within the yarn and those on each fibre surface, as presented in Fig. 3A. For plain, satin and basket weave, a bimodal pore size distribution is evidenced by mercury intrusion porosimetry with pore diameters between 10 and 100 μm. The prevalence of larger pores can be attributed to the crossed yarns overlaps and the fibre-to-fibre distances.[33] Smaller pores over the surface of the fibres can be tailored in the function of the CC treatment, during the manufacturing process and on additional treatments prior to system assembly (i.e., surface etching), which provide pore size distributions between 10 and 60 nm, through BET measurement, parallel the specific surface area of the pristine CC is increased.[34] Just as the porosity on the fibre influences the CC specific area, the porosity between and within the yarns directly influences the permeability of the material. The porosity-permeability relation is often described by the Kozeny-Carman equation where a fitting parameter, related to the CC structure, is required, the Kozeny-Carman constant. The anisotropy of some materials, like the CC, can be well correlated to the Tomadakis–Sotirchos (TS) model, which demands the use of parameters defining the flow in a 1-, 2- or 3D mode, and the fluid direction with respect to the porous media, either parallel or normal.[33] Concerning the cloth position, the parallel fluid direction is related to the in-plane permeability, while the normal associates a through-plane permeability, as shown in Fig. 3B. Several empirical models and experimental measurements have proven that the intrinsic in-

plane permeability (in the order of 1×10^{-11} m^2)[35] is higher than the through-plane permeability (in the order of 1×10^{-12} m^2)[11] in about one order of magnitude. The in-plane permeability can be reduced by orthogonal yarns placed in the primary flow direction.[33] Darcy's law is commonly used to empirically determine the permeability of a porous material. However, in some studiess of CC, a deviation from the linear trend between the flow rate and the pressure drop, dictated by Darcy's law, is seen.[36] In this respect, Darcy's law is valid when viscous forces cause the pressure drop at low flow velocities (creeping flow). For high flow velocities, the inertial forces dominate the pressure drop contribution and can be accounted for through the Forchheimer effect. The direct dependence of permeability on convective transport demands attention during the selection or design of an electrochemical system to achieve maximum performance. For example, in a fuel cell, forced convection can take advantage of the in-plane permeability as flow takes place through adjacent channels in interdigitated or parallel-serpentine fields. In the case of the through-plane permeability, the transport from the channel to the catalysts layer and *vice versa* demands attention. In the latter case, assembly conditions become important since permeability can be reduced on compression.[33,37]

Another important feature of CC is its tortuosity, which represents the ratio of the actual fluid path compared to a straight line between two points. The tortuosity influences several transport properties, such as effective diffusivity and conductivity. Commonly, effective properties are corrected by the Bruggeman correlation, based on spherical or cylindrical morphologies for isotropic porous media. When working with a cloth, the spherical correlation deviates the value of tortuosity by the correlated morphology; when using the

cylindrical correlation, the yarns overlapping is not captured.[11] A more realistic value of tortuosity necessitates the anisotropy of the CC being considered. From this perspective, an electrochemical cell incorporating CC electrodes presents a less tortuous pathway to liquid electrolyte along the in-plane direction compared to the through-plane direction, resulting in higher transport values for the less tortuous media, and lowered transport values for the more tortuous pathways. As proof of this statement, L. Xing and coworkers (2019)[35] demonstrated that the ratio of the in-plane and through-plane permeability, conductivity (electrical, ionic and thermal) and diffusivity is higher than one, even to 10 times higher for some properties. They suggested that neglecting the porous media's anisotropy can lead to performance overestimation of electrochemical systems. Some alternatives to predict the tortuosity of the CC are the TS model, for which a good fitting for the flow mode (1-, 2- and 3D) and direction (in-, through-plane) is mandatory, additional to the inclusion of the system compression effect; the mercury intrusion porosimetry, which captures the influences of fibre yarns, and the Lattice-Boltzmann (LB) modelling coupled with X-ray tomography. Rama and coworkers (2010)[38] presented the changes in properties related to cloth structure in the function of compression force (CpF) in a fuel cell. The changes in properties were related to three main changes in cloth structure: 1) the compaction of yarn fibres (CpF < 0.3 MPa), yarns elongation along the *x*- and *y*-direction (0.3 < CpF < 3.3 MPa), and yarns deformation as a consequence of the closing of void spaces (3.3 < CpF < 100 MPa). To complement the latter study, measurements on the compressive stress-strain relationship were used to identify differences in single or double CC layers. In both cases, the stress-strain behaviour was similar for most of the tested cloths, suggesting that the cloth properties will be conserved, even if the reactor operates with stacked cloth electrodes.[9] The properties listed in Table 2 demonstrate this tendency of the behaviour of the porous electrode. The in-plane permeability

shows a higher value for several CC samples than for through-plane permeability. For additional comparison, the carbon felt o paper gave even higher permeability values (in an unknown direction), at least for CC different to ELAT hydrophilic plain. These differences might be attributed to the tortuosity of each porous media, being lower for the woven electrodes than for the non-woven electrodes. In the case of the electrical resistivity, there is no clear tendency in the presented values. However, results reported by X.L. Zhou *et al.* (2016)[10] suggests that CC (ELAT hydrophilic plain) is less resistive than carbon paper (SGL10AA) either for the thickness of 200 and 400 μm, which were evaluated under the same operational conditions. It should be recognized that the listed values in Table 2 are not directly comparable to each other since the operating conditions involved different compression forces and porosities, in addition to some unknown directions for measurements.

From the above, it is important to highlight that transport properties differences between the in- and through-plane directions should be equally considered when designing an electrochemical system. It should be understood entirely to improve and optimize the operation design parameters. The electrical and chemical properties are conferred when the CC fibres surfaces are functionalised, particularly for electrocatalysis and adsorption. Surface functionalisation is attractive since the cloth structure receives a strategic, high loading of active materials. The principal techniques include physical, chemical/electrochemical, and thermal activation techniques, along with surface decoration with nanostructured catalyst particles, under a controlled mode for distributing active material onto the carbon fibre cloth, into spaces within its porous structure and into spaces between fibres.

Chemical and electrical properties

In essence, CC exhibits low surface energy, is hydrophobic and provides a chemically inert surface. Consequently, CF shows a low affinity for aqueous solutions and poor adhesion with polymers and resins, hindering the technical applications of CC electrodes.[39] Modification or activation of carbon fibres via physical, chemical, or thermal methods can increase their surface energy, improving the adhesion of composite materials and the material wettability, in addition to the natural increase of specific surface area. CC electrodes can be activated to the desired function or characteristic via the presence of heteroatoms on their surface, determining the acidic (tendency to accept hydrogen ions or valence electrons) or basic (tendency to donate hydrogen ions or a pair of valence electrons) character. The concentration of oxygen groups is related to an acidic character, which significantly impacts the adsorption capabilities of CC. The presence of oxygen groups can be promoted by oxidation of the carbon. On the other side, a basic character is related to π-electron resonance in carbon aromatic rings and nitrogen groups capable of binding with protons; this can be achieved by heat treatment or exposure to ammonia.[2]

M. Gineys and coworkers (2017)[3-4] obtained a CC electrode with enhanced adsorption capacity and kinetics by applying cathodic and anodic polarisation in a sodium sulphate electrolyte. They found significant differences between the cathodic and anodic treatments. The cathodic polarisation presented a preferential formation of phenolic groups on the CC surface, with negligible modifications on its pore structure. As opposed to anodic polarisation, where carboxylic, carbonyl, lactone, and quinone groups tend to form, a significant change of the pore structure resulted in a reduced pore volume, which can be attributed to fibre pore blocking. Not all types of activation induce structural changes in CC

electrodes. This enables the independent analysis of the surface functional groups and the enlarged specific surface area to determine which factor is responsible for the electrochemical system performance enhancement under study. Furthermore, CC can undergo a minor change in mechanical properties after activation.[40] A study made to improve the capacitive performance of the CC under wet chemical oxidation, showed that a large number of oxygen groups diminishes the CC conductivity. Consequently, adjusting the activation duration should optimize the ratio between carbon and oxygen groups on cloth surfaces.[41]

In addition to the activation of CC surfaces, the highly conductive carbon cloth offers itself as a suitable-based electrode to design binder-free decorated electrodes. This type of electrode provides short ion/electron diffusion paths. It can remove problems caused by contact resistance and dead volume generated by binders, an electronically conductive cohesive.[8] Surface functionalisation encompasses methods such as metal nanoparticle deposition,[5] electroactive polymers layers,[42] enzyme immobilisation,[43] and metal oxides, hydroxides,[6] and sulphides layers,[7] to name a few. Nanoparticulate carbon material can also be included to enforce the active material growth by promoting an effective interface. The active material content can be controlled in size, shape, and spatial distribution, mainly based on the modification time.

For example, CC coated with core-shell Au-Ag nanoparticles coated was used in a non-enzymatic hydrogen peroxide (H_2O_2) sensor as an oxidative stress biomarker, utilising an electroless deposition technique. An Ag-entrapped Au catalyst particle was obtained. Its size tends to grow homogeneously with deposition time; however, a disordered aggregation of

particles was found after a long deposition time, further diminishing the catalyst activity. A time-controlled catalyst surface homogeneity could be achieved for the H_2O_2 detection in blood serum, even in the presence of common physiological interferences, such as glucose, ascorbic acid, dopamine, and Na^+, Ca^{2+} and Fe^{2+} ions.[5] The polymer layer CC decoration can reach the development of high-performance pseudocapacitors. The polypyrrole nanowire arrays demonstrated that Faradaic reactions could accelerate charge storage via electropolymerisation at constant current density. The fabrication process warranted sufficient and controlled sites for the nanowire growth through the *p*-toluene sulphonate acid with increased current density.[1] Polymerisation of pyrrole can be improved by fabricating a continuous polyaniline layer prior to the polypyrrole nanotube network generation, followed by a second polyaniline layer over the nanotubes. This loaded, highly active material provides a large capacitance per unit area and high energy density electrodes for lithium-sulphur batteries.[44] During heavy metal ion uptake, layered double hydroxides (LDH) intercalated with different inter-layer anions on the CC surface give an interesting option for environmental remediation. The copper-chromium-LDH nanosheet intercalated with 2,3-dimercaptopropane sulfonate; and the nickel-chromium-LDH with diphenylamine-4-sulphonate were used for the superior selective adsorption of Hg^{2+}, Cd^{2+}, Pb^{2+}, Cu^{2+} and Zn^{2+} ions from water.[45-46] Independently of the final electrode application (i.e., sensors, batteries, bioremediation), Their high electrical conductivity and chemical stability allow CC electrodes to be tailored for particular applications. Optimisation of the CC surface microstructure can be reached via the growth of nanoparticles or films, ensuring good adhesion and chemical bonding to the CC surface, providing a higher substrate surface area for additional catalysis sites.

Cell design and reaction environment

In general, cloths have the versatility and flexibility to be constructed for any electrochemical application. CC can be fitted into various geometries for static- and flow-cells for multiple types of reactor. The porous CC material can combine the adsorption and desorption processes with electrode reactions, with a minor resistance to the liquid flow and is an attractive 3D porous material for electrocatalytic operations in liquid- and gas-phase systems. The used electrochemical cell types go from batch cells to continuous flow cells, with divided or undivided modes of operation. Classical three-electrode cell with CC working electrode (WE) is mainly employed for electroanalytical studies;[47] in bioelectrochemical systems, the batch-type benthic fuel cells (microbial fuel cell which uses organic matter present in marine sediment) are equipped with CC modified anodes to improve their performance.[48] Other researchers have used flow-through, flow-by and flow-across reactors for electrosynthesis of chemicals, removal of water contaminants and storage and energy conversion; cell configurations and features have been discussed.[49]

Cell design

In this section, some reports are referred to proposed electrochemical reactors utilising CC electrodes, as illustrated in Fig. 4. For example, the batch design of a typical three-electrode cell was used to evaluate a metal-free catalyst on CC for oxygen reduction reactions (ORR) in Fig. 4A. The authors take advantage of a facile chemical deposition method over the CC surface.[47] Another example is seen in the field of energy conversion, using benthic fuel cells, utilising the high surface area of CC electrodes and their biocompatibility in supporting biofilms growth in the corrosive marine environment, enhancing power production (Fig. 4B).[48] To take full advantage of the biocompatibility and large surface area of CC electrodes,

they must first be functionalized. The batch mode pf operation is often used today. In the flow-through configuration, a capacitive deionisation process was implemented to remove benzoic acid, polycyclic aromatics dyes, phthalic acid and nicotinic acid from wastewater using an ACC electrode within an electrosorption cell in Fig. 4C. The body of the reactor was built mainly of Teflon; a stainless-steel mesh in the centre of the channel acting as a base for the electrode and facilitating a homogeneous potential distribution when making electrical contact with the ACC. In this configuration, the ACC electrode (tow CC circles with a total mass of 40 mg) acted as a fixed bed working electrode by contacting a platinum wire.[50]

The filter-press cell allows the flow-by mode, as implemented by Cornejo & Nava in (2021), for the mineralisation of an antibiotic by the electro-peroxone process, using the CC as air-diffusion cathode, for the *in situ* oxygen peroxide production (Fig. 4D).[51] The cell was equipped with a Ti|IrSnSb-oxides anode (3 cm height and 8 cm length) and a 3D air-diffusion cathode, which was constructed by placing graphite felt of the anode dimensions, with a thickness of 0.25 cm (volumetric area of 651 cm^2 cm^{-3}). The commercial CC of 24 cm^2 was hydrophobized with PTFE. The cloth and felt were compressed during assembly. A stainless-steel window (3 cm × 8 cm × 0.23 cm, height, length, and thick, respectively) was used as a cathode current collector; polypropylene gaskets used as fluid distributors (3 cm high, 8 cm long, and 0.55 wide, between the electrodes and the air chamber), two type D turbulence promoters (plastic nets) were used; one was placed inside the air chamber and the other between the electrodes.[51]

The spiral wound microbial fuel cell (MFC), in Fig. 4E, was used to study hydrodynamics during its optimisation. Its main components (anode, cathode, and separator) were arranged as a sandwich and rolled up around a current collector axis, can be fed in co-flow, counter-flow, and cross-flow mode to enhance mass-transfer rates to utilise its high electrode surface area to volume ratio.[52-53] A commercial RFB is represented in Fig. 4F; the cell has a squared geometry with an interdigitated flow field. In this RFB, the complete monopolar plate (dimensions of 5.3 height × 5.3 length × 4 cm thick) with the flow channel was graphite (10.24 cm^2); the CC electrode (10 cm^2) was placed on top of the flow field. Instead of an ion exchange membrane, they used a cellophane film to separate the positive from the negative compartment, symmetrically assembled. In this RFB, the authors evaluated the flow patterns and residence time distribution to characterise the flow pattern of the cell.[54] Cell designs can use both dry and wet electrical connections. Dry connection considers the direct contact of the CC with the current collector (metal wire, foil or clips).[55-56] Wet connections are possible by using a polarised plate or mesh (i.e., graphite, metal foams or RVC) in contact with the CC.[51-52]

Reaction environment and porous electrode performance

The characterisation of the reaction environment allows analysing the design and performance of electrochemical reactors, leading to cell improvement design and the selection of operational variables to optimise the electrochemical reactor. Current density, electrolyte flow rate, temperature, and initial concentration of the electroactive species, favour mass transport and current and potential distributions, consequently enhancing the current efficiencies and improving energy consumption. On this basis, the porous CC

electrode can improve the mass transfer rate and the potential and current distributions by varying the volumetric area, the electrolyte flow rate, and the appropriate current density values. The variables to be analysed in this review are the fluid flow deviations, pressure drop, mass transport and current distribution carried out by experimental measurements and predicted by CFD simulations. For each analysed variable, published studies are addressed, encouraging the reader to identify areas of opportunity.

Non-ideal flow - A fundamental analysis in the characterisation of electrochemical reactors equipped with CC as an electrode is how the electrolyte flow is dispersed inside the cell. The residence time distribution (RTD) analysis is usually carried out to describe and determine the characteristics of the electrolyte flow dispersion, providing valuable information on electrolyte behaviour within the CC electrode and electrochemical cell. This analysis identifies undesirable flow patterns such as stagnant and recirculation zones, back mixing, and preferential flow paths. The RTD analysis allows the innovative design of components of the cell, including flow distributors and permits the selection of an adequate electrolyte flow rate to prevent non-ideal flow patterns.

Haeger *et al.* (2014) analysed the characteristics of the fluid in a compact spiral wound MFC, where ACC is used as anode and cathode.[54] They compared two electrode combinations under the same operational conditions; the first configuration (SW-1), a single sheet of ACC was employed as anode and cathode, while the second configuration (SW-2) employed two ACC sheets for each electrode; they separated the anode and cathode chambers with a cation exchange membrane. A NaCl tracer was introduced to the anode chambers to know the fluid behaviour. The solution conductivity was measured with periodic time intervals at the reactor

outlet until it was similar to the inlet solution conductivity. The obtained curve was a cumulative age distribution curve known as the *F-curve*, which indicates the tracer concentration ratio between the outlet and inlet flows over time. In Fig. 5A, the RTD analysis from the *F-curve* compares the ideal flow behaviour in a plug flow reactor with the actual flow behaviour in the SW-1 configuration, in which the differences between curves indicate the presence of dead space in the cell, the same was observed in the SW-2 configuration, in Fig. 5B. The RTD curves indicate that SW-1 presented a lower deviation than SW-2, with a dead space ratio of 20% *vs* 67%.[54]

In another study, the hydrodynamics characterisation was made for a redox flow battery with interdigitated flow fields. They obtained RTD curves with two different models: axial mixed dispersion (AMD) and plug dispersion exchange (PDE). Several flow velocities were analysed between 0.01 and 0.04 L min^{-1}. Fig. 5C and 5D show a comparison between the prediction of a model and the actual fluid behaviour. A close agreement at 0.03 and 0.04 L min^{-1}, unlike lower flow rates of 0.01 and 0.02 L min^{-1} (not shown), suggests the formation of stagnant zones. It is worth mentioning that the non-ideal flow deviations tended to disappear at a higher electrolyte flow rate. The stagnant phase and mass transport phenomena did not significantly affect the fluid pattern.[54] In the literature, few papers, such as Aparicio-Mauricio *et al*. (2020)[54] and Haeger *et al*. (2014)[52], analyse non-ideal flow inside electrochemical cells using CC electrodes, even when such a treatment is needed to guarantee good electrolyte flow dispersion, effective mass transport, and uniform current distribution, which determine the current efficiency and electrolytic energy consumption of the electrochemical processes. It is critical that a better understanding of the behaviour of the fluid within electrochemical cells is achieved via these theoretical and experimentally

validated studies, It remains important to develop theoretical models which can predict the hydrodynamic behaviour within electrochemical cells and establish mass transport correlations involving electrode reactions and current/potential distributions.

Fluid pressure drop **-** The pressure drop is an important parameter to be considered during the design and construction of flow fields, typically adjacent to the CC electrode, in RFB and FC. Cells should be designed to minimise pressure drop and allow the electrolytes to circulate more efficiently and reduce parasitic electrical losses due to pumping power demand.[57-58] V. Radhakrishnan and P. Haridoss (2011)[37] characterised the pressure drop in a fuel cell considering the interaction of flow fields design with CC properties, used as GDL, and the response of the system compression given by the components assembly. Apart from the changes in porosity and permeability of CC, the compression force can progress CC intrusion to the channel, resulting in partial cross-sectional area changes. A flow field with a higher channel hydraulic diameter (d_h = 4 × cross-sectional area / wetted perimeter[61]), from 1 to 1.5 mm, shows that the pressure drop in the system is reduced, from 60 to 20 mbar, at a flow rate of 0.5 L min^{-1}, maintaining a constant compression force (85% of its initial thickness). When the compression force increases from 85% to 75% of the initial thickness upon the CC, the pressure drop is pronounced. As an example, for a 1 mm d_h the pressure drop went from 60 to 75 mbar, at 85% and 75% compression. While for a 1.5 mm d_h the pressure drop went from 20 to 30 mbar. For a higher d_h, the CC intrusion is more noticeable, reducing the cross-sectional channel area. However, for the net pressure drop in the system, the high-pressure drop provoked by the lesser channel area can be attenuated by the fluid flow within the CC pores.[37] Zhou *et al.* in (2016)[10] present a study in an RFB with two carbonaceous electrodes,

paper and cloth. They observed that when using CC, the average fluid velocity is higher than the carbon paper, besides the pressure drop in the battery is lower when using CC (Fig. 6A). They concluded that the mass transfer in CC is better than in carbon paper, attributing this to the high permeability of CC, related to large pore size and low tortuosity. Park & Popov (2011)[59] also compared the behaviour of CC and paper on the water draining from a GDL in a PEMFC. They found that a higher liquid pressure is necessary to force the water to drain when using paper while the water stops flowing at minimum pressure. Contrary to the cloth response, which allowed the water to drain continuously, as a tandem effect of the oxygen flow within the high cloth porosity.[10]

The porous electrodes equipped in an electrochemical system will inevitably demand high pumping power, bringing along an improvement in the mass transport process. Some experimental results have suggested that the mass transfer coefficient (k_m) can be correlated to a power law function of pressure drop (Eq. 1), where empirical constants (a and b) vary with the cell geometry, electrode form and electrolyte flow conditions.[60]

$$k_m A_e = a\Delta P^b \quad (1)$$

The A_e variable refers to the volumetric electrode area. It is used to express the electrode characteristics quantitatively and serves to compare the properties of porous materials, such as CC. Another way to express a porous electrode area is the specific area, A_s.

$$A_e = \frac{A}{V_e} \quad (2)$$

$$A_s = \frac{A}{w} \quad (3)$$

where A, V_e and w are the surface area, volume and the weight of the porous electrode, respectively.[61]

The mass transfer coefficient and pressure drop correlation has been studied using flow-by reactors (i.e., FM01-LC). However, this can be extended to flow through reactor configurations since the fluid is forced to pass through all the electrode volume, and the pressure drops might have a more significant influence on its general performance. In general, pressure drop characterization is mainly found in FC and RFB. This type of hydraulic analysis is not widely reported in other application areas, with the exception of recent studies on metal meshes and foams by Arenas *et al.* (2020).[62]

Mass transport - The multimodal pore size offered by the CC, with large and small pores, attracts interest in many electrochemical applications, with demand on high mass transport regimes, since the fibres pattern gives rise to the large pores in the cloth promotes turbulence in the system's fluid. Coeuret and coworkers (2002), during mass transport studies on CC, found the double porosity feature in the material, in which only the outer surface works as an electrode.[56] On the other hand, Cloirec (2012) studied the structural parameters in terms of macrostructure and internal porosity of the cloth, and its relationship with the adsorption process on the fibres of the cloth, concluding that external mass transport predominates in CC electrodes.[63] In (2017), Zhou *et al.* exposed the issues of species transport in an RFB using CC electrodes. They stated that two main steps are involved in transporting the active species to the reactive surface: one corresponds to the transport of the active species from the cell entrance to the CC electrode pores, by yarns overlapping and fibre-to-fibre distance (macroscale level transport), and the second relates the transport within the CC pores to the reactive electrode sites of the cloth fibres, pores in each fibre surface (microscale level transport). After electrochemical reaction, a third step takes place when the products are

transported from the active sites back to the CC pores and then to the cell outlet.[64] An overall effective mass transfer coefficient ($k_{m,overall}$) is derived:

$$k_{m,overall} = \frac{1}{\frac{1}{k_{m,r}} + \frac{1}{k_{m,p}}} \quad (4)$$

where $k_{m,r}$ is the mass transfer coefficient for the macroscale level transport; and $k_{m,p}$ is the coefficient for the microscale level transport. In theory, $k_{m,r}$ under forced flow conditions might be evaluated through the dimensionless group correlation of Sherwood (Sh), Reynolds (Re) and Schmidt (Sc) in Eq. (5). In this expression, variables related to the electrode geometry and porosity, electrolyte properties, and operation conditions are involved through the a, b and c empirical constants.

$$Sh = aRe^{b}Sc^{c} \quad (5)$$

Since the empirical constants involve specific properties from a selected electrochemical system, equation (5) must be carefully applied inside the studied experimental variables interval. The extrapolation outside the characterised experimental limits must be avoided. Under the dimensionless group expansion and rearranging, and considering the case where the electrolyte is working at a constant temperature and a fixed electrode material, it is possible to reach the mean mass transport coefficient at the macroscale level in function of the volumetric flow rate, Q:[61,64]

$$k_{m,r} = aQ^{b} \quad (6)$$

For the microscale level transport, a mass transport correlation in the function of the *Re* number (representing the electrolyte flow rate) was presented by Xu & Zhao (2013) in equation 7, where the d_p is the pore diameter, and D is the diffusion coefficient of the electroactive species. The experimental arrangement was a vanadium-RFB with graphite felt

electrodes.[65] The applicable *Re* interval was limited under operatioal conditions. However, similarly, empirical constants can be obtained from each reactor design under the corresponding process conditions.

$$\frac{k_{m,p}d_p}{D} = 2 + 1.534Re^{0.912} \quad (0.3 < Re < 2.4) \tag{7}$$

Careful consideration must be given to the *Re* number; the study problem should be clear on the scale leve involved. That is, for a flow channel, the characteristic length is based on the hydraulic diameter (d_h), for a porous media, the pore diameter (d_p) is the characteristic length.[61] Leyva-Ramos and coworkers (2012) studied the external mass transport of organic compounds were affected by the molecular size of the organic compounds. Small molecules (size < 0.55 nm) governed the adsorption rate in the external mass transfer regime (around the cloth yarns). The model is represented by:

$$\frac{w\varepsilon}{\rho_p}\frac{dc}{dt} + w\frac{dw_{ads}}{dt} = wA_s k_m\left(c_{bulk} - c_{surf}\right) \tag{8}$$

where k_m is the external mass transfer coefficient, V is the electrolyte volume, ρ_p is the electrode density, w_{ads} is the mass of adsorbed solute and c_{bulk} and c_{surf} are the solute concentration in bulk and at the electrode surface. In equation (8), only a diffusional model of adsorption process is used. The approach assumes no concentration gradient in the fibre-to-fibre pores, resulting from fast diffusion. The first term on the left side of the equation refers to the solute accumulation in the pore volume of the CC, the second term on the left side refers to the accumulation of the solute on the surface of CC fibres. The term on the right hand side refers to the external mass transport speed. The model used by the authors[66] allowed the mass transfer coefficient in CC electrodes to be compared with experimental data. Fig. 6B shows a comparison of the experimental results and those obtained through the mathematical model described by the external mass transfer model (EMTM) in equation (9)

for the concentration decrease of pyridine (0.49 nm), phenol (0.53 nm) and naphthalenesulfonic acid, NSA (0.85 nm). The model agrees well with pyridine and phenol, but not for NSA. They concluded that the global adsorption rate of pyridine and phenol is mainly controlled by external mass transport. For the NSA, fibre-to-fibre diffusion was the controlling mechanism in the adsorption rate. This diffusion process is hindered by steric exclusion and pore obstruction by adsorbed molecules.

For a single electrochemical reaction controlled by mass transport, the limiting current can be related to the $k_m A_e$ product: [62]

$$k_m A_e = \frac{I_L}{zFcV_e} \quad (9)$$

where I_L is the limiting current given by the electrode, z is the number of electrons involved in the reaction, F is the constant of Faraday and c is the bulk reactant concentration.When the electrode surface area is determined by the BET technique, the physical adsorption process, generally using N_2, can lead to higher values than the available area for an electroactive species. On another hand, the geometrical area estimation based on ideal cloth fibre shapes (i.e., cylindrical), lengths or diameters would result in a skewed performance of the cell. An alternative to obtaining the $k_m A_e$ product directly from I_L, is to determine the fractional conversion in a plug flow reactor.[61]

Studies on the characterisation of mass transport in CC electrodes are scarce, even when such an analysis provides kinetic information to enable the electrochemical cell to be well designed and scaled-up.

Potential and current distribution - Few articles about potential and current distributions in CC electrodes are available in the literature, even when these porous electrodes exhibit

uneven current distribution. Coeuret *et al.* in (2002) carried out studies on the effect of electrical conductivity on the potential distribution in plain (CC-3257) and twill CC (CC-3872) types.[56] In Fig. 6C, the CC-3257 shows the potential drop *vs* current intensity, for different lengths of CC (10.5, 20, and 38 cm), it is evident that potential drop increases with the cloth length, highlighting that the slope, attributed to the apparent global resistance, decreases at high current intensities. This resistance reduction indicates the potential distribution in the CC-electrolyte interface, which might be attributed to conduction between neighbouring fibres. On the other hand, the potential drop *vs* current intensity in the CC-3872 in Fig. 6D shows a linear resistance over a broader current density range. The latter behaviour is attributed to the number of fibres in the yarns, CC-3872 having 16 times more fibres than CC-3257. The type of CC, particularly the fibre content that makes up the cloth, determines the potential drop in this electrode. Hence, selecting a cloth type and its experimental characterisation utilising polarisation curves before the application is necessary. A selection criterion for a CC electrode should be achieving the least electrical resistance over a wide range of current density. In the literature, it is difficult to find information on the percolation of the potential at the CC-electrolyte interface and the dynamic reaction front. Such studies would provide crucial information, such as the apparent conductivity of the CC-electrolyte interface, which is necessary for mathematical modelling and simulation of the potential and current distributions in flow cells equipped with CC electrodes.

Modelling and simulation - Modelling and simulation work allows the description of hydrodynamics, mass transport, and current distribution within electrochemical reactors with porous electrodes.[67-69] Although such studies are necessary when designing reactors equipped with CC electrodes; few such studies are in the literature. Zhang *et al.* in (2020)[70]

used the lattice Boltzmann model in conjunction with experimental measurement of electrochemical performance and X-ray computed tomography in an RFB to understand coupled mass transport and electrochemical reaction processes, simulating the flow of electrolytes, the transport of species, and charges.[70] In the simulation of transport species, these authors used the equation:

$$\frac{\partial c}{\partial t} = \nabla \cdot (D_i \nabla c_i) - \nabla (c_i v) + \nabla \left[\frac{z_i F c_i D_i}{RT} \nabla \varphi_e \right] \quad (10)$$

where c_i, D_i and z_i are the concentration, diffusion coefficient, and charge of the electroactive species, v is the linear velocity of the electrolyte, R is the universal gas constant, T is the temperature and φ_e is the electrolyte potential. The first, second and third terms from the right side in equation 10 refer to the transport of species by diffusion, convection, and migration, respectively. For the charge transport simulation, the governing equation for the potential field in the carbon electrode is:

$$\nabla \cdot (\kappa_s \nabla \phi_s) = 0 \quad (11)$$

where κ_s is the electrical conductivity of CC. The potential field in the electrolyte can be obtained as:

$$\nabla \cdot [\kappa_e \nabla \varphi_e + F \sum_i D_i \nabla c_i] = 0 \quad (12)$$

where κ_e refers to the electrolyte conductivity. It is defined as:

$$\kappa_e = \frac{F^2}{RT} \sum_i z_i^2 D_i c_i \quad (13)$$

Zhang's group carried out simulations with CC, finding that the microstructure of this electrode is very important in the concentration overpotential. They observed that the CC has good performance in terms of pressure drop, reducing the operating costs. Park and Li (2008)[71] also used the LB model to simulate the multiphase flow phenomenon in the

anisotropic gas diffusion layer of a PEMFC, obtained from microscopic images. The LB equation led to Stokes and Brinkman's equations to model the porous structure of CC. They simulated the CC as a void space, facilitating the movement of liquid drops in a porous medium. The results agreed well with the experimental results, finding that the orientation of the fibres in these cells is significant since the anisotropic medium directly influences its permeability.[71]

A study by Messaggi *et al.* (2018)[72] modelled a vanadium RFB in 3D, mainly using the Navier-Stokes, Brinkman, and Nernst-Planck equations. The authors analysed the hydrodynamics in the flow field and the porous electrode in a serpentine and an interdigitated geometry. These authors found that the serpentine-shaped geometry has higher performance and more significant pressure drops over the interdigitated; however, they observed that the interdigitated geometry achieves a more homogeneous distribution regarding the flow and mass fields.[72] In the latter and most modelling studies of porous media, the Bruggeman equation is used for CC since it relates the free-stream properties to the actual mass transport in a porous media, in function of the porosity and tortuosity of the medium. When the Bruggeman equation is not valid for a specific porous media (e.g., carbon paper), measurement of the MacMullin number is recommended, as it considers the tortuosity and porosity dependence for the geometric model of the actual porous media.[73]

Aparicio-Mauricio *et al.* in (2020) performed the modelling of the hydrodynamics and mass transport of an RFB, focusing mainly on obtaining the flow patterns and RTD within the battery.[54] The squared batterie's geometry with an interdigitated flow field used CC electrodes. The equations used by the authors were Navier-Stokes and Brinkman. The RTD

analysis was carried out using the convection-diffusion equation. Fig. 7A shows the theoretical *F-curve* obtained from the simulation, compared against the experimental RTD at different flow rates, being well correlated. In Fig. 7B, the velocity field developed within the CC electrode shows that the highest velocities are under the ribs, a characteristic behaviour of interdigitated fields; furthermore, in the insets near the inflow and outflow zones, stagnant and low-velocity zones can be appreciated at the outermost lateral ribs and under the channels of the interdigitated design. The authors pointed out that any slight difference in the length of the channel would cause an expansion in the RTD. The simulation results' velocity profiles within the CC at different flow rates are presented in Fig. 7C and correspond to the auxiliary line in Fig. 7B. It is demonstrated that the fluid velocity increases at higher volumetric flow rates; at a sufficiently high flow rate (i.e., 0.04-0.03 L min^{-1}), the velocity values show significant variations between the channels. This variation in velocity decreases at lower flow rate. The CFD study helps to understand the behaviour of RFBs when equipped with CC electrodes.

The modelling and simulation of cells of any type and, in this case, equipped with CC electrodes help predict the cell's behaviour, allowing to know the performance of the cell and the possible optimisation if necessary, finding weaknesses mainly in the design of the cells. Therefore, modelling and simulation can be used in both cases to improve the design and performance of already built cells and to design a new electrochemical cell. The modelling and simulation of electrochemical cells that use CC electrodes are implemented in batteries and FC applications, mainly finding hydrodynamics, mass transfer, and current distribution studies. These analyses allow obtaining the best operational conditions for the reactor, such as current density, flow rate, temperature, and initial concentration of electroactive species,

among others. It is worth mentioning that this section was focused on the part of commercial software for predicting the hydrodynamic, mass transfer and potential distribution behaviour of the electrochemical cells equipped with CC electrodes through different parametric models or fundamental equations. The parametric models presented herein, equations 5-9, describe any electrochemical process limited by mass transport occurring in the CC. On the other hand, the solution of the fundamental equations 10-11 require boundary conditions involving faradaic currents for specific electrochemical reactions.[60]

Applications

The continually growing application of electrochemical techniques in kinetics, sensing, synthesis, environmental remediation, energy storage and conversion demands the development and use of efficient electrodes, with a desirable performance in terms of low overpotentials and excellent durability and stability. Commonly, a wide variety of electrocatalysts are supported on three-dimensional (reticulated vitreous carbon or metal foams) or two-dimensional (graphite, platinum, steel) substrates. The latter presents the disadvantage that catalytic layers detach from the substrate in gas evolution reactions or extreme media environments of alkalinity or acidity, as an example, resulting in decreased activity and durability.[74] Therefore, the self-supporting substrates, which are supposed to be free from detachment and serve as the catalytic surface and electrode, offer a promising active and durable electrode material.[75] Currently, the CC allows the cultivation or growth of active materials directly in their fibres surface, automatically enhancing the cloth surface area.[187] Another advantage of carbon cloth is the flexible matrix provided by its woven fibre tows, which allows the facile integration in different devices, maintaining its high mechanical strength and electrochemical stability.[76]

Electrode kinetics and sensing

The "easy" surface functionalization of carbon cloth electrodes improves electron transport kinetics. The presence of surface heteroatoms on CC has shown various advantages for its applications in different fields. For example, oxygen-containing groups can enhance the oxygen evolution reaction (OER).[77] While the nitrogen-containing groups work towards hydrogen evolution reaction (HER).[78] Diminishing their overpotential and Tafel slope with respect to the bare CC, as listed in Table 3. Also, the adsorptive properties can be modified when coupling the CC with electroactive materials. As the electroactive materials can be cultivated directly on the cloth fibres surface,[79-82] inducing a parallel structural change, the CC provides a viable option for electrochemical sensors. As discussed in the review made by Torrinha and Morais (2021),[76] the CC allows designing devices with outstanding analytical performance due to the high surface-to-volume ratio accompanied by the 3D architecture giving rise to a vast quantity of electroactive sites.[76] From this point of view, it is essential for the designing workgroups to wonder if the surface characteristics of the fibres are the best means of maximising the performance of the sensors. Probably, it is just as beneficial to focus the attention on the structural characteristics of the CC and analyse how these significantly influence its transport properties. It opens a broader path towards optimising the proposed sensors since there is a lack of reports on these structural properties' advantages on the electrochemical sensors.

Electrosynthesis

The synthesis of chemical products, organics or inorganics, is a daily life constant, either in the development of technics or in the manufacturing process, until reaching the final user.

The electrochemical methods cover plenty of areas related to the production of chemicals able to compete with conventional technologies when environment regulations, time and easiness of production, and cost of the process are on the table.[83]

Inorganics - Following the same concept of using CC as catalyst support, palladium catalysts were used for H_2O_2 production, emphasising the control oxidation state of palladium (PdO and Pd^0) and the hydrophilicity of the carbon fibre surface.[84] The hydrophilicity facilitates the access of the metal precursor to the interior of the fibre-to-fibre pores during impregnation using water; in contrast, having a hydrophobic bare carbon fibre, the very low affinity for polar solvents will allocate the metal precursor at the external surface of the CC.[85] When attention is paid to the large- or pilot-scale production process, gas-diffusion electrodes based on CC have shown stunning results. Filter-press type electrolysers take advantage of CC to feed reactants in the gas phase to produce different chemical products, whether liquid or gaseous.[86] Foller (1986)[87] patented an electrolyser to produce gaseous hydrogen chloride and aqueous alkali metal hydroxide. The latter was equipped with a semi-hydrophilic catalyst impregnated CC electrode. The most critical feature was the anode's shielding ability to prevent the gaseous product from entering the electrolyser instead of sending it to the back of the electrode to get the valuable chemical.[87] Furthermore, the high production rate could be attained through the CCs high surface functionalised area and the enhanced mass transport through the forced convection within the porous electrode.[88] The hydrophilicity of CC can facilitate functionalisation. When the applications of CC rose the large-scale production process, the CC is presented as a suitable electrode since it allows the feeding of the reactant through the electrode and avoids the leakage of the product through this same electrode. It is necessary to acknowledge that a closer view to the woven CC and fine structure (on a

microscale length) would offer additional advantages. For example, the uncompressed functionalised CC would allow efficient use of the new active sites within the fibre-to-fibre spaces once the electrode is fitted in a system under compression? How would the functionalisation step behave if the cloth were more tightened and had higher areal weight? Where will the active sites generate the most, in yarn intersections or within them with the change of the areal weight? Or, in the case of a gas diffusion electrode, the selected cloth types can send incoming reactants in one direction different to the outcoming products?

Organics - CC electrodes are suitable cathode materials during microbial electrosynthesis. Where the electricity serves as source reduction of CO_2 to carbon organic molecules used as fuels, in this respect, Zhang and coworkers (2013)[89] analysed different treatments on CC substrates to improve the rate of fuel production through the electrode-microbe electron transport. The main goal was to positively charge the CC surface since the untreated CC was reported as neutral.[89] Among the natural biopolymers (chitosan, amino and hydroxyl group) and metal nanoparticles (gold, palladium and nickel) used for enzyme immobilization, the former presented a better performance, showing a 7-fold fuel production rate. In contrast, the metal nanoparticles gave around a 5-fold production rate; both compared to the untreated CC. These performances were attributed to the high active surface area and biocompatibility of the electrode along with the catalytic activity resulting from the given treatment. Another interesting organic application is propionate degradation,[90] acetoclastic methanogenesis,[91] metabolism of alcohols and volatile fatty acids,[92] among others.[93-96] These studies have shown that the conductive CC promotes the direct interspecies electron transfer mechanisms, offering a potential improvement in anaerobic methane generation compared to the interspecies hydrogen transfer. The anaerobic methanogenesis and other systems with batch

reactors designs may experience mass transport limitations, which can be overcome by adopting a continuous-flow reactor. For example, the use of CC as gas diffusion cathode for the conversion of carbon dioxide into liquid fuels, like isopropanol and long-chain hydrocarbons (C9-C10), presents itself more convenient than converting solubilized carbon dioxide in aqueous solutions that produce methane and C2 hydrocarbons, related to low carbon dioxide solubility and high overpotentials.[97-99]

Environmental remediation and water treatment

The use of CC as support in 3D electrodes has been proposed both as new technology and an excellent tool in water treatment. In electrochemical advanced oxidation processes (EAOP) for water treatment, CC helps the oxidation of emerging persistent organic pollutants in CO_2 and water.[100-101] The CC as a porous electrode in the cathodic electrodeposition of heavy metals allows the recovery of metals in a state of zero oxidation and the reuse of treated water, making it a sustainable process.[102] In addition, CC has been used in the desalination of water during capacitive deionization processes.[103]

Electrochemical advanced oxidation processes - EAOP for water treatment involve some of the most successful applications utilising CC electrodes. 3D electrodes of CC is commonly used as a cathode for the *in situ* production of H_2O_2 in the presence of O_2 in an acidic solution (Eq. 14) through the Fenton reaction, EF (Eq. 15).[104-106] The H_2O_2 as the central reactant interacts with ferrous ion (Fe^{2+}) catalyst to form hydroxyl radicals ($^{\bullet}OH$), which is a strong and non-selective oxidizing agent capable of converting any persistent organic pollutant (R) to carbon dioxide (CO_2) and water (H_2O) (Eq. 16).[100-101,104,107-108] The incorporation of UVA radiation from an ultraviolet lamp or solar radiation favours the reduction of carboxylic

complexes formed by the degradation of organic pollutants (Eq. 17), which enhances the oxidising power, giving rise to the processes called photoelectro-Fenton (PEF) and solar photoelectro-Fenton (SPEF), respectively. On the other hand, the electro-peroxone process is based on the reaction of ozone with electrogenerated H_2O_2 to yield $^{\bullet}OH$ (Eq. 18).[109-111] The electro-peroxone process works well in a wide range of pH 0-9, while homogeneous processes based on electro-Fenton operate at pH 3.

$$O_2 + 2H+ + 2e^- \rightarrow H_2O_2 \quad (14)$$

$$H_2O_2 + Fe^{2+} \rightarrow Fe^{3+} + {}^{\bullet}OH + OH^- \quad (15)$$

$$R + {}^{\bullet}OH \rightarrow CO_2 + H_2O \quad (16)$$

$$[Fe(OH)]^{2+} + h\nu \rightarrow Fe^{2+} + {}^{\bullet}OH \quad (17)$$

$$2O_3 + H_2O_2 \rightarrow 2{}^{\bullet}OH + 3O_2 \quad (18)$$

The electrosynthesis of H_2O_2 is carried out using gas-diffusion electrodes consisting of CC with a polytetrafluoroethylene (CC/PTFE) film to promote hydrophobicity. In these electrodes, the oxygen is typically supplied from an external air compressor on the back of the hydrophobized CC side, and oxygen reacts *in situ* at the electrolyte-oxygen-CC/PTFE interface. Experimental electrolysis of electro-peroxone and electro-Fenton processes are performed in laboratory three-electrode cells in the presence of poorly defined flow and mass transport by magnetic stirring (with volumes from 30 to 500 cm^{-3}). However, the most compelling studies are performed in continuous filter-press type cells, where fluid flow is better defined, and the hydrodynamics favours mass transport.[51,104] Many papers consider the deposition of carbon nanotubes, graphene, and metallic catalysts to increase the catalytic activity during the reduction of oxygen to produce H_2O_2.[112-114]

Márquez *et al.* (2020)[115] carried out a comparative study of EF and PEF processes for the removal of methyl orange azo dye, in which a filter-press type electrochemical reactor was used (Fig. 4 D), equipped with graphite felt and CC cathode. The results show efficiencies of total organic carbon removal to both processes of 66% and 94%, respectively.[115] Coria *et al.* (2018) experimentally analysed the antibiotic levofloxacin's mineralisation using the SPEF process in a pre-pilot plant using a CC/PTFE gas diffusion cathode.[101] Their results showed the effectiveness in the production of H_2O_2 and the complete mineralization of the pharmaceutical drug, highlighting sunlight as a source of photons that allowed the decomposition of refractory complexes and reduced energy consumption. Cornejo *et al.* (2021) studied the degradation of the textile dye Acid Violet 19 using electro-peroxone processes in the cell shown in Fig. 4 D equipped with a CC-PTFE-graphite felt cathode and a $Ti|IrO_2$ anode.[116] The hydrogen peroxide was formed in the cathode. This process permitted the complete decolouration of the treated water. Despite the wide use of EAOP in water treatment, almost all the investigations found in the literature are limited to experimental analysis and few published investigations refer to the modelling of current distribution, potential and mass transfer, which turn out to be critical in the simulation of electrochemical processes, and thus be able to characterize the reaction environment and optimize these electrochemical processes.

Metal ion removal from wastewater - The increase in the industrialization of certain sectors such as metal-mechanic, tanneries, battery producers, paper industry, as well as fine-scale and tonnage chemicals, represent a source of contaminated water that has resulted in lower

water quality, particularly by heavy metals discharged directly or indirectly to surface water bodies and aquifers. This represents a severe pollution problem since they are toxic, non-biodegradable, and, in addition, can accumulate in living organisms such as plants and animals.[117-122] Different metal ions such as Cu (II), Cd (II), Pb(II), Ag (I), Hg (II), Co (II), Ni (II), Zn (II) and Cr (VI) have been removed using porous electrodes (i.e., carbon and graphite cloth).[45,123-127]

Extensive studies have shown that CC can be used as 3D cathodes because they have a large volumetric area and are excellent at successfully removing heavy metals from dilute solutions compared to plate electrodes, which are generally used to treat high concentrations of heavy metal ions.[128] Lou *et al.* (2019)[123] employed the CC with MoS_2/Bi_2S_3 deposits as photocatalysts for the degradation of the hexavalent chromium (Cr(VI)) present in wastewater, achieving photocatalytic removal of 75.5% of Cr(VI) from a solution with an initial concentration of 50 mg L^{-1}, after 100 min, with a flow rate of 1.0 L min^{-1}. Therefore, the versatility of CC in removing and recovering metals from dilute solutions is important for industrial applications. Shamsayei *et al.* (2020)[45] demonstrated that electrodeposition of Cu-Cr on CC is an excellent technique for the removal of heavy metals from aqueous solutions. The results showed great capacity for the adsorption of metals with efficiencies close to 100% in solutions that contained an initial concentration of 100 mg L^{-1} of each metal in individual solutions of 20 mL.[45] However, when performing mixing tests of two metals, the efficiency was affected, showing that CC with Cu-Cr deposits has selectivity in multicomponent solutions in the following order Hg (II) > Cd (II) > Pb (II) > Co (II) > Ni (II) > Zn (II). The capacity of graphite cloth electrodes has been used to remove copper, cadmium, and mercury ions from a deoxygenated solution by electrodeposition. Fig. 8 shows

a set of curves obtained for the removal of cupric ions from synthetic solutions at three different initial concentrations (2.2×10^{-4}, 1.4×10^{-4}, and 7×10^{-5} M Cu^{2+}) and at a constant potential of -0.7 V *vs* SCE. The removal percentages of copper as a function of the electrolysis time are presented, reaching current efficiencies of 85, 90 and 95%, respectively.[129] It is worth mentioning that no papers show a systematic experimental characterization of the flow velocity and current density on the metal removal efficiency in flow cells equipped with CC electrodes (i.e., evaluating the current efficiency and electrolytic energy consumption). There are also no papers showing CFD simulations of hydrodynamics, mass transport and current distribution during metal electrodeposition, even when these phenomena are crucial to obtain the best operating conditions to be applied to the electrolysis or for designing an *ad hoc* electrochemical reactor.

Capacitive deionization - CDI is an emerging technology that plays a critical role in water desalination. It has recently been used to treat wastewater contaminated with heavy metals and persistent organic compounds. CDI is based on the capacitive principle and is characterized by low energy consumption (from 0.13 to 0.59 kW h m^{-3}) since it operates at low voltages (0.6 - 2.0 V).[103,130-131] The electrodes used in CDI are mainly porous carbon materials such as activated carbon, activated carbon cloth, graphene, carbon nanotubes, and carbon nanofibres. In 2011, Lee *et al.* evaluated the use of CC as a substrate for elaborating layered electrodes of ion exchangers for advanced membrane CDI.[132] Sulfonation and amination were used to form cationic and anionic exchange layers. They observed that the use of CC could improve ionic selectivity and solve the problems of high contact resistance.

Furthermore, the electrode showed an 83% removal efficiency of 100 mg L^{-1} NaCl with an energy consumption of ≈23.1 kW h. Beyond being used as a 3D electrode in desalination processes, CC has been employed in different studies to remove dyes from wastewater and the removal of heavy metals from groundwater, where they take advantage of its multiple characteristics.[133-134] Thamilselvan *et al.* (2018)[135] investigated the effect of three different dyes (amido black 10B, eosin yellow, and methyl violet) on the CDI of a saline solution using ACC as an electrode. A 40-60% dye removal efficiency was achieved in a flow cell. On the other hand, Liu and Wang (2020)[136] used an ACC electrode/graphene oxides for the removal of Co^{2+} and Cs^{+} contained in an aqueous solution with a concentration between 5 to 20 mg L^{-1} and applying a constant potential of 1.2 V, the results showed efficiencies of 40.8 and 37.9% for concentrations of 5 mg L^{-1}, in the removal of Co^{2+} and Cs^{+}; respectively. They also observed that by increasing the initial concentration to 20 mg L^{-1}, the removal efficiencies decreased to 17 and 23.2% during the removal of Co^{2+} and Cs^{+}, respectively.[136] On the other hand, CC has been used as an adsorbent material for removing contaminants from water; however, the results obtained have not been satisfactory due to the low specific surface of CC (between 1 to 30 m^2 g^{-1}) compared to that provided by activated carbon (from 500 to 1000 m^2 g^{-1}).[137-139] Therefore, recently, the ability of CC with metal oxide compounds for use as electrodes in CDI has been studied. In 2012, Myint and Dutta produced activated CC electrodes with zinc oxide nanowires for the desalination of the brackish water of 100 mg L^{-1} of NaCl at 2 mL min^{-1} and applying a potential of 1.2 V during CDI. They obtained an efficiency of 34%.[140] However, in a recent study by Kyaw *et al.* (2020)[141] deposited SiO_2 nanoparticles in ACC and used them as electrodes in CDI for desalination of brackish water with 200 mg L^{-1} of NaCl showing efficiencies of 73% applying a potential of 1.8 V, in addition, the investigation revealed that the surface coating of nanoparticles of SiO_2 in

activated CC electrodes prevents oxidation of the surface. Although the application of CC-oxides has not only been limited in its application for desalination, the CC-oxides has also been applied in the removal of heavy metals. Such is the case of Kyaw *et al.*, with CDI, by modifying the adsorption properties of CC with zinc oxide nanoparticle coatings.[141] The metal ion removal process to constant cell potential (1.8 V) showed the capacity to remove Pd(II) and Cd(II) from dilute solutions (0.5 mM of initial concentration) either individually or mixed, with removal efficiencies of 33, 29 and 35% for Pd (II), Cd (II) and Pd (II)-Cd (II) solution, respectively. Although CC has been widely used as a 3D electrode for the removal treatment of various contaminants in synthetic brackish water, its application to practical water treatment is still very limited.

Energy storage and conversion

When considering the growing global demand for energy today and the parallel requirement for the use of sustainable and green technologies, renewable solar and wind energy sources appear to be limited by fluctuations in energy production. As an alternative to this limitation, energy storage and electrochemical conversion technologies can be employed by means of the CC as a common electrode substrate for both types of technology. To improve their power and reduce their cost.

Static batteries

Secondary batteries are preferred over single-use primary ones due to their capacity to be recharged. Rechargeable lithium-ion batteries dominate the market due to their high energy and power capacity and long service life. However, concern over the availability of Li resources, which is not sufficient to meet the growing demand for Li-ion batteries, in addition

to concerns about safety and the environment when they are damaged, encourages the relentless search for alternative batteries.[142] A suitable alternative is sodium,[142] aluminium[143] and zinc[144] ions, for its abundance on earth. Intercalation/deintercalation processes lead to the volume expansion of the active metals in the battery, resulting in a decrease in capacity. Thus, carbon fibres are ideal hosts to tolerate volume change and inhibit dendrite formation, contrary to metal electrodes' behaviour.[145-147] The degree of crystallinity in carbon fibre electrodes can markedly influence the performance of battery electrodes. It is common to find hard carbon (non-graphitisable) and soft carbons (graphitisable). Hard CC (p.e., pitch-based CF) offers the advantage of being more robust in surface exfoliation, which relates the irreversible losses in the first cathodic scan; also, during the Li-ion intercalation process, hard carbons give more cyclical stability than graphite anodes (soft carbons).[148-149] In addition, CC shows the ability to achieve higher gravimetric and volumetric energy densities than soft carbons with almost the same cell voltage.[145] Considering the limited volume change of lithium alloys within a carbon fibre electrode, N. Imanishi (1993) demonstrated that the intercalation/deintercalation process was better with a low degree of crystallinity of the carbon fibre.[150] Furthermore, if the orientation of the carbon layers has a 3D texture, the diffusion of lithium ions towards the interior is improved without destroying it. All batteries present an irreversible process intrinsically involved in the intercalation of metal ions, known as the "formation of a solid-electrolyte interface" making battery life a critical issue.[151] A Na-ion battery with a CC anode and a metallic cathode was tested to understand the fading ability during the long cycle process, and the most significant deterioration was found in the electrolyte and the metallic counter electrode, in contrast to the CC structure, which did not show sign of destruction. However, it presented a solid-electrolyte interface within it.[28] This effect followed a mathematical model proposed by Pinzon and Bazant (2013),[151] in which

the solid-electrolyte interface grows homogeneously through the porous electrode, with a moderate non-uniformity when subjected to high temperatures and extreme load conditions. As an alternative to diminishing the loss of capacity, several works focus on avoiding the formation of the solid-electrolytic interface by passivation of the CC surface, giving a selective performance towards the metal ion and obstructing the passage of the electrolyte solvent.[148,152-153] Attaining a high specific energy capacity is one of the main goals for using batteries in any field. Despite the low theoretical specific capacity of bare CC (20 mA h g^{-1}),[154] surface treatments for the introduction of heteroatoms[155-157] and the binder-free growth of compounds over the CF surfaces and within the porous structure (fibre-to-fibre distance) allow the CC electrode to be competitive against graphite (with a theoretical specific capacity 372 mA h g^{-1}),[158] carbon felts, [159] and carbon powder/binder electrodes,[160] either metal- or air-batteries. As shown in Fig. 9, the CC based batteries reflect higher specific capacity than non-CC based batteries. For example, for a Li-ion battery using CC, the maximum registered specific capacity (in the figure) is around 1000 mAh gr^{-1} at a specific discharge current of 1000 mA gr^{-1}, against the Li-ion battery on graphite with 150 mA h g^{1} at 100 mA g^{-1}. This trend of non-CC materials to be lower in capacity is attributed to the ability of the open structure of CC to facilitate electrocatalysis of the ORR and OER kinetics.[161-162] Currently, several studies have emphasised the diverse structural forms of 3D CC (considering the fibre-to-fibre spaces in yarns and the fibre surface pores) can increase the contact between active material and electrolyte, decrease the diffusion distance from ions and electrons and high performance. Contrary to this, Mckerracher and coworkers observed that during Al-ion intercalation, the process is easier on large smooth surface areas of graphite or carbon paper than on porous CC.[143] When selecting the best electrode for a battery, many interrelated

parameters should be considered, including the influence of the electrolyte and electrode surface in the shuttle-ion process together with the effect different types of CC porosity.

Redox flow batteries

At the beginning of RFB development, especially in vanadium-RFB, porous carbon electrodes were reported to show signs of deterioration during the first couple of charging cycles, mainly in the negative electrode.[164] Several modification processes increase carbon material stability, surface area, and chemical activity enhancement, resulting in an attractive material for these technologies.[165] Several CC surface modification techniques have been reported to improve the electroactive sites when increasing the active surface area. As mentioned above, activation, functionalization or decoration methods can be explored. To address the issues related to the manufacturing and operational cost of the RFB, catalytic surfaces need to be focused on the operating parameters, which can hinder the market penetration due to the power-related costs that represent near 60% of the total.[64] CC porous electrodes can positively impact costs during RFB operation by means of their structure-related properties. Its high permeability and low tortuosity enhance the inflow of electroactive species, exposing them to many active sites for electrochemical reactions. Equally, its positive effect on mass transfer is observed.[166] In (2016), Zhou *et al.* analyzed the transport properties of CC and carbon powder in an interdigitated RFB flow field,[10] reporting that the CC allowed higher flow velocities to be achieved with almost the same pressure drop along with the cell for both electrodes. The lower resistance of CC led to a better electrochemical performance.[64] The balance between the power density performance and the pumping losses obtained with CC was related to the compensation between mass-transport power and pumping, which suggested that further increase in the flow rate would

lead to an increase in the performance, unlike carbon paper or felt electrodes, which limit the flow at maximum rates without improving power.[167] Zhang and collaborators (2020)[70] carried out a mathematical study, via the LB model, related to the transport phenomena within woven CC and non-woven carbon fibres. The CC gave better results, in which there was an absence of stagnant fluid, a more uniform distribution of concentrations inside the porous domain and a lower activation overpotential compared to carbon paper. The main difference between the analysed materials was the pore size distribution, as shown in Fig. 10, where the Freudenberg and SGL papers show a narrow distribution of pore sizes, with one dominant peak around 20 μm for the former, and two dominant peaks around 10 and 100 μm for the latter. The size distribution is random in the SGL paper and goes from 0 to 160 μm. On the other hand, the CC presented a narrower pore size distribution with a maximum peak at 15 μm. A relationship between the pore size distribution and pressure drop within the domain shows that CC imposes less resistance to fluid flow than Freudenberg and SGL papers. Even though SGL has a larger proportion of larger pores (see Fig. 10), the random accommodation of fibres in the paper may lower the fluid flow by the increased tortuosity of media. For the Freudenberg paper, the random fibres distribution, in addition to its small pore sizes, the fluid flow is not so favourable as its competitors. In LB simulation, the change in media porosity was not considered, assuming that the used compression ratio (10-20%) does not change the porous media structure significantly but enhances the yarn fibres contact to improve electrical conductivity. This feature should be considered in a physical experimental arrangement since, as measured by P. Rama (2011),[9] in the general compaction of cloth fibres stage (with a compression force below 0.3 MPa), the diminution of porosity is near 18% with respect to the no-compressed CC.[30] For this reason, a trade-off must be found between the improvement in the electrical conductivity of the porous medium and the impact it will have

on the transport properties of electrolyte. The battery performance relies not only on electrode design or selection but also on the flow field geometry, cell configuration and operational parameters. A quinone-ferrocyanide RFB with interdigitated flow fields incorporated six different plain-CC types to identify the limiting factors on the full RFB performance.[9] In general, the ohmic resistance presented itself as the principal loss in the cell due to the flow field and the electrode thickness, followed by the pumping losses, which becomes significant only under extreme electrode compression (point of zero permeability). Both can be minimized under an electrode compression between 50-60% to reach an optimum reduction in electronic resistance. On the other hand, the mass transport effect had minimal effect under the tested flow rates and operations conditions; and the charge transfer presented a minor factor in the overall polarization effects. The used CC-types were obtained from different suppliers. Half of the samples were made of three-filaments bundles (twisted and untwisted) in each longitudinal and transverse yarns, and the other half of samples with a one-filament bundle in each yarn. The benchmark RFB performance is represented by the one-filament bundle group (CFCE, Elat and Zoltek) among the six samples. A filament diameter of 8 μm, an average area-specific resistance of 0.32 Ω cm^2 and a weave periodicity of 20, 20 and 17 cm^{-1}, respectively. Compared with the three-filaments bundles group, where the cloth with twisted filaments bundles presented lower specific resistances (0.7 Ω cm^2) and high weave periodicity (18 cm^{-1}), and the untwisted filaments bundles gave the highest specific resistance (4.5 Ω cm^2) with lower weave periodicity (<5 cm^{-1}). In these last samples, the diameter of the filaments is similar (9-10 μm). Despite that each cloth property was not directly correlated to the RFB performance, it can be suggested that a new path towards CC optimization can be traced since it was possible to see that cloth structure-property directed by their

manufacturing process might improve reactor performance in addition to the valuable insights into selecting electrode types to existing electrochemical systems.

Supercapacitors

The dependence on the electrochemical performance of supercapacitor electrode materials has drawn much attention to CC. Supercapacitors possess a double-layer electrical capacitor and pseudo-capacitor characteristics.[168] The voltage of the system and the specific capacitance of the electrodes determine the energy density of the supercapacitors. Subsequently, the voltage can be optimized through the selected electrolyte and the combination of the electrode materials for the cathode and the anode. On the other hand, the specific capacitance can be enhanced through material engineering, modifying its intrinsic properties.[169] The CC, often used as a support structure for active materials, allows a high mass loading and better utilization of electrode area to enrich the capacitance of the electrodes since bare CC gives a relatively low area-specific capacitance ($\approx 3.7\times10^{-5}$ F cm^{-2}).[156] Furthermore, this material allows the exclusion of binders during the doping process, reducing interfacial resistance and enhancing electrochemical reaction rates.[31] The incorporation of polyaniline and carbon nanotubes, or reduced graphene oxide onto the CC surface, has led to the enhancement of a real specific capacitance to 4.04 F cm^{-2} [44] and 0.71 F cm^{-2}, [170] respectively. Compared to the capacitance of bare CC capacitance, a significant improvement in specific surface area resulted from the microscale architecture of each electrode.

The addition of redox electroactive species to the surface is another option to raise the charge storage capacity of CC electrodes. The cycling stability of those systems can be assured by

adding anthraquinone or its derivatives to perform a covalent bonding between the redox group and the CC surface.[171] A supercapacitor with 1,5-diamninoanthraquinone designed by L. Juanli *et al.* (2020)[172] reached 0.921 F cm^{-2} at 1 mA cm^{-2} and achieved up to 20000 charging/discharging cycles. The stability of the covalent bonding is highly superior to the polyaniline modified CC, where the latter reports stability up to 5000 cycles.[31] Metal oxide colloids have reported to show an excess capacity, beyond their theoretical values, using the contribution of the cation (Ni^{2+}) and anion (Fe^{3+}) redox paradigms,[173] giving an energy density of 353 W h kg^{-1} ; at 2250 W kg^{-1} power density, the cycling stability rachieved 10000 cycles at a specific current of 30 A g^{-1}. Many other dopants deposited on the CC surface to obtain a high capacitance value include metal carbides, nitrides,[157] sulfides,[174] oxides,[175] oxyhydroxides,[176] and the introduction of heteroatoms (O-, N-, and H- groups).[177] However, challenges are still present since the selection of symmetrical or asymmetrical devices offers an extensive range of power output possibilities, given that asymmetric SC allows overcoming the energy storage limitations imposed by symmetric capacitors.[178]

Ovhal and coworkers (2020) proposed an asymmetric SC with high electrical charge storage and improved charge transfer and electrochemical properties utilising an anode, a faradaic electrode, and a cathode as a pseudo-capacitor. They took advantage of the CC to directly grow nickel hydroxide and carbon nanotubes on the grooves and crests of CF providing an additional active area for charge storage. The resultant areal and specific capacitance was reported to be 1.248 F cm^{-2} and 3987 F g^{-1} for the anode and 0.278 F cm^{-2} and 928 F g^{-1} for the cathode. The SC assembly exhibited 27.7 kW kg^{-1} power density at an energy density of 132 W h kg^{-1}, with a wide potential window of 1.8 V, this assembly being superior to similar proposed asymmetric SCs.[179] The control over the grooves and crest dimensions in the CC

architecture is expected to provide a higher storage energy performance but the influence of the CC structure on the electrochemical area presented by carbon fibres has not been studied in detail.

Fuel cells

The power output and the life of the FC are a function of multiple factors, including the design of the flow channels, operating conditions, components properties, among others.[180] The essential participation of the gas diffusion layer GDL occurs during the distribution of active species and the removal of excess water to and from the electroactive catalyst layer (CL), respectively. Also, the GDL provides a pathway for transporting electrons and serves as mechanical support for the CL and membrane.[181] The CC and carbon paper are common materials selected as GDL. The structural differences between these woven and non-woven carbon materials were numerically studied by Y. Wang *et al.* (2007)[182] under the assumption of an isotropic media. They identified that in high humidity conditions the cell performance is enhanced by CC due to its low tortuosity allowing easy liquid water to drain from the CL. In comparison, carbon paper has better performance in low humidity conditions since its high tortuosity imposes additional resistance to the water draining and prevents membrane dehydration due to low humid gas flow.[182] This is a good starting point to improve the FC designs; however, it is essential to consider that in high-aspect-ratio components, the influence of anisotropy in the transport properties plays a fundamental role. In this respect, mathematical modelling would provide valuable results. Gao *et al.* (2020)[183] studied the microscopic pores formed in the CC using a 3D stochastic reconstruction technique. They adopted the geometric cloth parameters, resulting in elliptic yarns conformed by multiple filaments (representing the CF) in a plain weave pattern (representing the CC). The CC

permeability and tortuosity behaviour were analysed to the variations in the radius of the cloth fibres and the cloth porosity, which later were used to compute a momentum transport problem. Within the cloth, the main flow path went through the larger pores, concentrated in the overlap zone between the yarns; either the radius of the fibres or the cloth porosity was changed. However, with an increment in porosity (resulting in the CF quantity diminution) from 0.68 to 0.81, the fluid velocity tends to be more uniform; the water accumulates with a porosity near 0.9. On the other side, when the filament radius was between 2-3 μm, the velocity was nearly uniform; for a radius over 3.5 μm, the water starts to accumulate, in this case, the quantity of fibres in the yarn is reduced too. It can be concluded that a loose weave with a high transversal section to the fluid pass is not beneficial since it could propitiate the cell flooding and mass transport limitations towards the reactive gas.[183] Considering this, the structure compression might benefit the fluid distribution since the clamping pressure could unite the fibres and diminish the media porosity while enhancing the electric contact between yarn fibres, as discussed in the properties section.[184] Another method to manage water within an FC is the PTFE CC impregnating, which could change the material porosity. However, the effects of PTFE on the CC have been extensively studied elsewhere.[185-187] In addition to the GDL architecture, several variables are related to a FC performance, including the design of flow fields (cross-sectional channel areas, rib/channel width relation), the operating condition like relative humidity, cell temperature, the cell configuration in which the feeding mode (co-flow, counter-flow) or cell position (vertical, horizontal), several studies have been conducted to understand the mentioned variables interrelation to which reader is referred.[188-189] Despite these proven techniques to enhance performance, it is recommended that cloth features are scrutinised to identify possible influences of the weave yarns in favour of the fuel cell design.

Microbial fuel cells - The electrogenic capacity of some bacteria is deployed in some MFC to produce electricity from organic waste. It is possible to have simultaneous energy generation and bioremediation in this sense.[190] In other MFC, the electrodes involve enzymes immobilised on porous carbon; both types of MFC have been modelled and reviewed.[191] Indeed, CC is commonly used as a substrate for oxygen reduction at the cathode and biofuel oxidation at the anode.[192] The CC modification methods strive for the activation of the surface, the introduction of metal oxides,[193] polyelectrolytes,[194] or the preparation of carbon composites.[190] The power generation in a benthic MFC was compared using different polyaniline coated anodes: CC-polyaniline and graphite plate-polyaniline. The CC-polyaniline generated almost two times the power generated by graphite plate-polyaniline, 11.14 mW m^{-2} and 5.52 mW m^{-2}, respectively.[48] The authors attributed the result to the extensive electrolyte access into the 3D anode structure generated by the polyaniline layer, which reduced the anode internal resistance. In a bare CC MFC, significant diffusion limitations were found.[194]

Despite the moderate electrical resistance of CC, the material can demonstrate high stability in MFC, indirectly showing the substrate's metabolic ability.[192] The tight network of woven yarns allow a uniform growth of the biofilm on the surface which, in the case of scaling up to an industrial level, can be considered a robust solution in the design of multilayer electrodes.[195] Blanchet and coworkers (2016) found that the differences in surface area between carbon felts and CC have an insignificant influence on the electrochemical performance due to the detected biofilm pattern, where the thickness of the biofilm is the inverse of the microbial volume ratio. The CC had a biofilm thickness of 80-120 μm and a

microbial volume ratio of 39.3%, compared to a biofilm thickness of 200-800 μm and a microbial volume ratio 16.3% in the carbon felt suggested that the CC surface was fully accessible to microorganism growth, leading to a compact uniform biofilm, in contrast to the carbon felt biofilm, in which a larger penetration compensated for the low volume ratio.[195]

In practice, the benefits and limitations of an electrode material should be considered in a balanced fashion to propose the best cell configuration. In this respect, B. Fu and collaborators (2019)[190] designed a composite anode of granular activated carbon and CC (GAC/CC) to combine the high mechanical strength and the low internal resistance. The composite was tested on a flow-through reactor, obtaining an enhanced power production and reduction in chemical oxygen demand, attributed to the reduced overall internal resistance and mass transfer enhancement due to the flow velocity, compared to a static reactor with the same composite anode. Figure 11 shows the maximum power density achieved from various MFC. A comparison between bare and modified CC is revealed when the anodes of each MFC were subjected to different surface treatments. Notably, these were measured in different types and sizes of cells, using various electrolytes and microbial cultures. Nevertheless, this comparison indicates the positive impact of the different anode surface treatments compared to the bare CC. The high surface area of CC benefits microorganism growth and the differences between cloth and felt demonstrated that CC concentrates the organism growth at the electrode surface, making it suitable for large-scale applications. Despite this, differences dictated by manufacturing features of a fresh CC electrode (including weave pattern, number of filaments and weigh per unit area) have not been correlated to the organism's growth and to the power density achieved by an MFC. Such studies could improve electrode design and significantly improve reactor performance.

Summary

CC electrodes offer high electrical conductivity, good mechanical strength, reasonable chemical resistance, and a wide potential range. Attention to weaving of cloth can further improve properties. This can be related to the ordered patterns, possible by suitable cloth design, resulting in high porosity with a pore size distribution ranging from nm to μm and characterised by controlled void spaces at yarn intersections, the fibre-to-fibre spaces in the yarns and the pores over the surface of carbon fibres. Given the porosity and low tortuosity conferred by weave patterns, anisotropic transport properties related to the fluid permeability, such as electrical, ionic and thermal conductivity as well as diffusivity should be considered when designing the electrochemical system or when selecting the electrode material. For the same reason, transport properties can be enhanced or hindered depending on the direction that fluid (gaseous or liquid) will move within the CC, since when an electrochemical system is compressed (e.g, to improve the electrical conductivity with the CC contact with the current collector, or when leakage of fluid should be avoided) the CC porous structure will deform in the compression force direction, resulting in a negative impact for the properties in that deformation direction. The bare CC is commonly treated or functionalized to improve or tailor the CC substrate to a specific desired function, to later adapt CC electrodes to a static or flowing electrolyte cell, for a wide range of applications. In general, most applications take advantage of the high surface area given by the CC, followed by the high porosity, permeability and low tortuosity, presenting a promising electrode substrate. However, the cloth offers additional features that seem not considered or depth studied until now; let us refer to the cloth patterns, the thickness of yarns (filament counts) and cloths, yarn tightness (which impacts in weight per unit area) and ease of handling. Few studies have focused on characterisation of cloth structure and its impact on properties. The latter can lead to

overcoming electrochemical limitations by improving the design of CC electrodes, especially if it is accompanied by the characterisation of reaction environment in these cells in terms of fluid flow, mass transport and potential and current distributions. The absence of such preliminary studies prior to the application can result in poor current efficiency and costly electrolytic energy consumption. The few studies that attempt a rigorous characterisation of the reaction environment in electrochemical cells from experimental and CFD approaches tend to be found only in PEMFC and RFB applications.

Recommendations for further research and development

Several aspects of carbon cloth electrodes deserve further study to improve their performance in electrochemical technology:

1. More detailed and quantitative studies of the structure of the CC electrodes suited for electrochemical use and the influence structure has on the transport properties of the CC electrodes.
2. More detailed and documented CC specifications (in terms of filament counts and areal weight) to be suitable for the desired applications.
3. Design of novel electrochemical cells using CCs in flow-by, flow-through and flow-across mode with their correspondent characterisation of the reaction environment in terms of fluid flow and mass transport together with analysis of current and potential distributions in the applications of electrosynthesis of organics and inorganics and in the environmental remediation and water treatment.

Acknowledgements

The authors thank the University of Guanajuato for financial support through project No. CIIC 167/2021. M.I.L and A.A.M. acknowledge CONACYT for awarded scholarships Nos. 624647 and 894987.

List of symbols

Symbol	Meaning	Units
A	Electrode surface area	m^2
A_e	Volumetric electrode area	m^{-1}
A_s	Specific electrode area	$m^2\ g^{-1}$
a, b, c	Constants in equations (1), (5) and (6)	-
c	Concentration	mol m^{-3}
c_{bulk}	Bulk concentration	mol m^{-3}
c_{surf}	Surface concentration	mol m^{-3}
d_h	Hydraulic diameter	m
d_p	Mean pore diameter	m
D	Diffusion coefficient of electroactive species	$m^2\ s^{-1}$
F	Faraday constant	C mol^{-1}
I_L	Limiting current	A
k_m	External mass transfer coefficient	m s^{-1}
$k_{m,overall}$	Overall mass transfer coefficient	m s^{-1}
$k_{m,r}$	Mass transfer coefficient for macroscale level transport	m s^{-1}
$k_{m,p}$	Mass transfer coefficient for the microscale level transport	m s^{-1}
Q	Volumetric flow rate	$m^3\ s^{-1}$
R	Universal gas constant	J K^{-1} mol^{-1}
t	Time	s
T	Temperature	K
v	Linear velocity of electrolyte	m s^{-1}

V_e	Volume of the porous electrode	m^3
w	Weight of porous electrode	g
w_{ads}	Mass of adsorbed material in porous electrodes	g
z	Electron stoichiometry in the primary electrode reaction	Dimensionless

Subscripts

i	Electroactive species	-

Greek

ε	Porosity	Dimensionless
ϕ_s	Potential of solid (electrode) phase	V
φ_e	Potential of liquid (electrolyte) phase	V
κ_e	Electrical conductivity in the liquid (electrolyte) phase	$S\ m^{-1}$
κ_s	Electrical conductivity in the solid (electrode) phase	$S\ m^{-1}$
ρ_p	Density of the porous electrode	$g\ m^{-3}$

Dimensionless groups

F(t)	Dimensionless cumulative function
Re	Reynolds number, $Re = vd_e/\nu$
Sc	Schmidt number, $Sc = v/D$
Sh	Sherwood number, $Sh = k_m d_e/D$

Abbreviations

ACC	Activated carbon cloth
ACF	Activated carbon fibres
AMD	Axial mixed dispersion
EAOP	Electrochemical advanced oxidation process
BET	Brunauer-Emmet-Teller
BSU	Basic structural unit
CC	Carbon cloth
CDI	Capacitive deionization
CF	Carbo fibre
CFD	Computational fluid dynamics
CL	Catalyst layer
CpF	Compression force
EF	Electro-Fenton
FC	Fuel cell
GAC	Granular activated carbon
GDL	Gas diffusion layer
LB	Lattice-Boltzmann (model)
LDH	Layered double hydroxides
MFC	Microbial fuel cell
NSA	Naphthalenesulphonic acid
PAN	Polyacrylonitrile
PDE	Plug dispersion exchange
PEF	Photoelectro-Fenton

PEMFC	Proton exchange membrane fuel cell
PTFE	Polytetrafluoroethylene
RFB	Redox flow battery
RTD	Residence time distribution
RVC	Reticulated vitreous carbon
SC	Supercapacitor
SPEF	Solar photoelectro-Fenton
TS	Tomadakis-Sotirchos (model)
WE	Working electrode
3D	Three dimensional
2D	Two dimensional
1D	One dimensional

References

1. Z. Huang, Y. Song, X. Xu and X. Liu, *ACS Appl. Mater. Interfaces*, **7**, 25506 (2015).
2. M. S. Shafeeyan, W. Daud, A. Houshmand and A. Shamiri, *J. Anal. Appl. Pyrolysis*, **89**, 143 (2010).
3. M. Gineys, R. Benoit, N. Cohaut, F. Béguin and S. Delpeux-Ouldriane, *Chem. Eng. J.*, **310**, 1 (2017).
4. K. Kordek, H. Yin, P. Rutkowski and H. Zhao, *Int. J. Hydrog. Energy*, **44**, 23 (2019).
5. N. Gowthaman, P. Arul, J. J. Shim and S. A. John, *Appl. Surf. Sci.*, **495**, 143550 (2019).
6. B. Hai and Y. Zou, *Sens. Actuators B Chem.*, **208**, 143 (2015).
7. M. Hua, T. Chen and H. Ma, *Appl. Energy Mater.*, **2**, 4316 (2019).
8. I. Shakir, Z. Almutairi and S. Shar, *Ceram. Int.*, **47**, 17427 (2021).
9. A. A. Wong and M. J. Aziz, *J. Electrochem. Soc.*, **167**, 110542 (2020).
10. X. L. Zhou, T. S. Zhao, Y. K. Zeng, L. An and L. Wei, *J. Power Sources*, **329**, 247 (2016).
11. J. T. Gostick, M. W. Fowler, M. D. Pritsker, M. A. Ioannidis, L. M. Behra, *J. Power Sources*, **162**, 228 (2006).
12. E. Fitzer, D. D. Edie and D. J. Johnson, in *Carbon Fibres Filaments and Composites*, 1st ed., J. L. Figueiredo, C. A. Bernardo, B. R. Baker and K. J. Hüttinger, Editors, p. 3-72, 119-146, Springer, New York (1989).
13. P. F. Grieger, *Study Papers on the auxiliary electrode*, published by the Electrochemical working group of the interagency advanced power group, PIC-BAT 209/9 section I-II (1965).
14. X. Huang, *Materials*, **2**, 2369 (2009).
15. A. P. Mouritz, in *Introduction to Aerospace Materials*, p. 303-337, Woodhead Publishing (2012).

16. B. A. Newcomb and H. G. Chae, in *Handbook of properties of textile and technical fibres*, A. R. Bunsell, Editor, p. 841-871, Woodhead Publishing (2018).
17. M. Suzuki, *Carbon*, **32**, 577 (1994).
18. K. K. Chee Ho, H. Qian and A. Bismarck, in *Wiley Encyclopedia of Composites*, 2nd ed., L. Nicolais and A. Borzacchiello, Editors, p. 1-11, John Wiley & Sons, Inc. (2012).
19. C. Minke, U. Kunz and T. Turek, *J. Power Sources*, **342**, 116 (2017).
20. D. D. Chung, in *Carbon Fibre Composites*, D. D. Chung, Editor, p. 65-78, Butterworth-Heinemann, Boston (1994).
21. J. Y. Chen, in *Activated Carbon Fibre and Textiles*, J. Y. Chen, Editor, p. 4-13 (Chapter: 1), 249-251 (Chapter 10), Woodhead Publishing Series in Textiles (2017).
22. W. J. Farnborough, T. L. Farnhan, P. M. Bentley, R. M. Crookham, A. Farnborough and W. W. Farnborough, *United States Patent Office*, Patent No. 3 541 582, (1970).
23. K. Homma and A. Nishimura, *United States Patent Application Publication*, Publication No. US 2005/0085157 A1, (2005).
24. Y. Matatov-Meytal and M. Sheintuch, *Appl. Catal. A-General*, **231**, 1 (2002).
25. R. T. Ogulata and S. Mavruz, *Fibres Text. East. Eur.*, **18**, 71 (2010).
26. I. Jahan, *Adv. Res. Text. Eng.*, **2**, 1-1018 (2017).
27. A. Lund, N. M. van der Velden, N. K. Persson, M. M. Hamedi and C. Müller, *Mater. Sci. Eng. R-Rep.*, **126**, 1 (2018).
28. C. Bommier, D. Leonard, Z. Jian, W. F. Stickle, P. A. Greaney and X. Ji, *Adv. Mater. Interfaces*, **3**, 1600449 (2016).
29. J. Pollitt, *J. Text. Inst. Proc.*, **40**, 11 (1949).
30. F. T. Pierce, F. Inst. P. and F. T. I., *J. Text. Inst. Trans.*, **28**, 45 (1937).

31. P. Liu, J. Yan, Z. Guang, Y. Huang, X. Li and W. Huang, *J. Power Sources*, **424**, 108 (2019).

32. I. Natalie, F. Anura, A. Sonja and L. W. Taylor, *Res. J. Text. Appar.*, **21**, 342 (2017).

33. K. M. Tenny, A. Forner-Cuenca, Y. M. Chiang and F. R. Brushett, *J. Electrochem. Energy Convers. Storage*, **17**, 041010 (2020).

34. R. Wang, L. Yinshi and Y. He, *J. Mater. Chem. A*, **7**, 10962 (2019).

35. L. Xing, Y. Xu, P. K. Das, B. Mao, Q. Xu, H. Su, X. Wu and W. Shi, *Chem. Eng. Sci.*, **195**, 127 (2019).

36. J. P. Feser, A. K. Prasad and S. G. Advani, *J. Power Sources*, **162**, 1226 (2006).

37. V. Radhakrishnan and P. Haridoss, *Mater. Des.*, **32**, 861 (2011).

38. P. Rama, Y. Liu, R. Chen, H Ostadi, K. Jiang, Y. Gao, X. Zhang, D. Brivio and P. Grassini, *Fuel Cells*, **11**, 274 (2011).

39. M. Kahoush, N. Behary, A. Cayla, B. Mutel, J. Guan and V. Nierstrasz, *Appl. Surf. Sci.*, **476**, 1016 (2019).

40. L. Zeng, T. Zhao and L. Wei, *Adv. Sustain. Syst.*, **2**, 1 (2018).

41. X. Liu, W. Xu, D. Zheng, Z. Li, Y. Zeng and X. Lu, *J. Mater. Chem. A*, **8**, 17938 (2020).

42. H. Shi, F. Zhu, X. Zhou, H. Li, F. Yang, X. Zhang and J. Liu, *J. Electroanal. Chem.*, **840**, 328 (2019).

43. R. Jayabalan, M. Sathishkumar, E. S. Jeong, S. P. Mun and S. E. Yun, *Bioresour. Technol.*, **123**, 686 (2012).

44. L. Dong, G. Liang, C. Xu, W. Liu, Z. Z. Pan, E. Zhou, F. Kang and Q. H. Yang, *Nano Energy*, **34**, 242 (2017).

45. M. Shamsayei, Y. Yamini, H. Asiabi and M. M. Khataei, *Appl. Clay Sci.*, **196**, 105747 (2020).

46. H. Asiabi, Y. Yamini, M. Shamsayei and E. Tahmasebi, *Chem. Eng. J.*, **323**, 212 (2017).

47. E. Asadian, S. Shahrokhian and A. Iraji Zad, *Int. J. Hydrog. Energy*, **45**, 1890 (2020).

48. O. Prakash, A. Mungray, S. K. Kailasa, S. Chongdar and A. K. Mungray, *Process Saf. Environ. Protection*, **117**, 11 (2018).

49. L. F. Castañeda, F. C. Walsh, J. L. Nava and C. Ponce de León, *Electrochim. Acta*, **258**, 1115 (2017).

50. E. Bayram, C. Kizil and E. Ayranci, *Water Sci. Technol.*, **77**, 848 (2018).

51. O. M. Cornejo and J. L. Nava, *Sep. Purif. Technol.*, **254**, 117661 (2021).

52. A. Haeger, C. Forrestal, P. Xu and Z. Jason, *Bioresour. Technol.*, **174**, 287 (2014).

53. A. D. Le, S. B. Beale and J. G. Pharoah, *Fuel Cells*, **15**, 27 (2015).

54. G. Aparicio-Mauricio, F. A. Rodríguez, J. J. Pijpers, M. R. Cruz-Díaz and E. P. Rivero, *J. Energy Storage*, **29**, 101337 (2020).

55. R. M. Kakhki, *Arab. J. Chem.*, **12**, 1783 (2019).

56. F. Coeuret, E. Oliveira and E. Bezerra, *J. Appl. Electrochem.*, **32**, 1175 (2002).

57. R. M. Darling and M. L. Perry, *J. Electrochem. Soc.*, **161**, A1381 (2014).

58. M. L. Perry, R. M. Darling and R. Zaffou, *J. Electrochem. Soc.*, **53**, 7 (2013).

59. S. Park and B. N. Popov, *Fuel*, **90**, 436 (2011).

60. F. F. Rivera, C. Ponce de León, F. C. Walsh and J. L. Nava, *Electrochim. Acta*, **161**, 436 (2015).

61. D. Pletcher and F. C. Walsh, in *Electrochemical Technology for a Cleaner Environment*, J. D. Genders and N. L. Weinberg, Editors, Chapter 3,The Electrosynthesis Company Inc., Lancaster, New York (1992).

62. L. F. Arenas, C. Ponce de León and F. C. Walsh, *J. Electrochem. Soc.*, **167**, 023504 (2020).

63. P. Le Cloirec, *Chin. J. Chem. Eng.*, **20**, 461 (2012).

64. X. L. Zhou, T. S. Zhao, L. An, Y. K. Zeng and L. Wei, *J. Power Sources*, **339**, 1 (2017).

65. Q. Xu and T. S. Zhao, *Phys. Chem. Chem. Phys.*, **15**, 10841 (2013).

66. R. Leyva-ramos, R. Ocampo-Perez and J. Mendoza-Barron, *Chem. Eng. J.*, **183**, 141 (2012).

67. T. Doherty, J. G. Sunderland, E. P. Roberts and D. J. Pickett, *Electrochim. Acta*, **41**, 519 (1996).

68. J. M. Bisang, K. Juttner and G. Kreysa, *Electrochim. Acta*, **39**, 1297 (1994).

69. J. S. Newman and C. W. Tobias, *J. Electrochem. Soc.*, **109**, 1183 (1962).

70. J. A. Trainham and J. Newman, *J. Electrochem. Soc.*, **124**, 1528 (1977).

71. D. Zhang, A. Forner-Cuenca, O. O. Taiwo, V. Yufit, F. R. Brushett, N. P. Brandon, S. Gu and Q. Cai, *J. Power Sources*, **447**, 227249 (2020).

72. J. Park and X. Li, *J. Power Sources*, **178**, 248 (2008).

73. M. Messaggi, P. Canzi, R. Mereu, A. Baricci, F. Inzoli, A. Casalegno and M. Zago, *Appl. Energy*, **228**, 1057 (2018).

74. M. J. Martínez, S. Shimpalee and J. W. Van Zee, *J. Electrochem. Soc.*, **156**, B80 (2009).

75. M. Tamilselvan, T. V. Sreekanth, K. Yoo and J. Kim, *Appl. Surf. Sci.*, **529**, 147077 (2020).

76. M. Balogun, W. Qiu, H. Yang, W. Fan, Y. Huang, P. Fang, G. Li, H. Ji and Y. Tong, *Energy Environ. Sci.*, **9**, 3411 (2016).

77. A. Torrinha and S. Morais, *Trends in Analyt. Chem.*, **142**, 116324 (2021).

78. C. Ningyan, L. Qiang, T. Jingqi, X. Yurui, A. M. Asiri, H. Jiang, Y. He and S. Xuping, *Chem. Commun.*, **51**, 1616 (2015).

79. C. Zhang, S. Bhoyate, M. Hyatt, B. L. Neria, K. Siam, P. K. Kahol, M. Ghimire, S. R. Mishra, F. Perez, F. and R. K. Gupta, *Surf. Coat. Tech.*, **347**, 407 (2018).

80. J. Li, Y. Liu, C. Liu, W. Huang, Y. Zhang, M. Wang, Z. Hou, X. Wang, M. Jin, G. Zhou, X. Gao, Z. Zhang and J. Liu, *Chem. Commun.*, **56**, 305 (2019).

81. C. Mahala, R. Sharma, M. D. Sharma and S. Pande, *ChemElectroChem*, **6**, 5301 (2019).

82. Y. Zhang, Y. Zhang, L. Li, J. Chen, P. Li and W. Huang, *J. Electroanal. Chem.*, **861**, 113939 (2020).

83. T. Zhe, R. Li, Q. Wang, D. Shi, F. Li, Y. Liu, S. Liang, X. Sun, Y. Cao and L. Wang, *Sens. Actuators B-Chemical*, **321**, 128452 (2020).

84. F. F. Rivera, C. Ponce de León, J. L. Nava and F. C. Walsh, *Electrochim. Acta*, **163**, 338 (2015).

85. D. Gudarzi, W. Ratchananusorn, I. Turunen, T. Salmi and M. Heinonen, *Top. Catal.*, **56**, 527 (2013).

86. D. Gudarzi, W. Ratchananusorn, I. Turunen, M. Heinonen and T. Salmi, *Catal. Today*, **248**, 69 (2015).

87. P. C. Foller and R. T. Bombard, *J. Appl. Electrochem.*, **25**, 613 (1995).

88. P. C. Foller, *United States Patent Office*, Patent No. US 4 595 469 A, (1986).

89. S. Hrapovic, M. F. Manuel, J. H. Luong, S. R. Guiot and B. Tartakovsky, *Int. J. Hydrog. Energy*, **35**, 7313 (2010).

90. T. Zhang, H. Nie, T. S. Bain, H. Lu, M. Cui, O. L. Snoeyenbos-West, A. E. Franks, N. K. Nevin, T. P. Russell and D. R. Lovley, *Energy Environ. Sci.*, **6**, 217 (2013).

91. Y. Xu, M. Wang,Q. Yu and Y. Zhang, *Bioresour. Technol.*, **302**, 122796 (2020).

92. J. Li, L. Xiao, S. Zheng, Y. Zhang, M. Luo, C. Tong, H. Xu, Y. Tan, J. Liu, O. Wang and F. Liu, *Sci. Total Environ.*, **643**, 1024 (2018).

93. Z. Zhao, Y. Zhang, Y. Li, Y. Dang, T. Zhu and X. Quan, *Chem. Eng. J.*, **313**, 10 (2017).

94. V. A. Burboa-Charis and L. H. Alvarez, *I. J. Energy Res.*, **44**, 10996 (2020).

95. S. Chen, A. E. Rotaru, F. Liu, J. Philips, T. L. Woodard, K. P. Nevin and D. R. Lovley, *Bioresour. Technol.*, **173**, 82 (2014).

96. R. Jia, D. Sun, Y. Dang, D. Meier, D. E. Holmes and J. A. Smith, *Bioresour. Technol.*, **298**, 122547 (2020).

97. Y. Lei, D. Sun, Y. Dang, H. Chen, Z. Zhao, Y. Zhang and D. E. Holmes, *Bioresour. Technol.*, **222**, 270 (2016).

98. G. Centi, S. Perathoner, G. Winè and M. Gangeri, *Green Chem.*, **9**, 671 (2007).

99. G. Centi and S. Perathoner, *Topics in Catalysis*, **52**, 948 (2009).

100. M. Gangeri, S. Perathoner, S. Caudo, G. Centi, J. Amadou, D. Bégin, C. Pham-Huu, M. J. Ledoux, J. P. Tessonnier, S. D. Su and R. Schlögl, *Catal. Today*, **143**, 57 (2009).

101. G. Coria, T. Pérez, I. Sirés, E. Brillas and J. L. Nava, *Chemosphere*, **198**, 174 (2018).

102. T. Pérez, G. Coria, I. Sirés, J. L. Nava and A. R. Uribe, *J. Electroanal. Chem.*, **812**, 54 (2018).

103. C. Huang and Y. Su, *J. Hazard. Mater.*, **175**, 477 (2010).

104. B. Han, G. Cheng, Y. Wang and X. Wang, *Chem. Eng. J.*, **360**, 364 (2019).

105. G. Coria, T. Pérez, I. Sirés, E. Brillas and J. L. Nava, *J. Electroanal. Chem.*, **757**, 225 (2015).

106. M. A. Oturan and E. Brillas, *Port. Electrochim. Acta*, **25**, 1 (2007).

107. E. Brillas, I. Sirés and M. A. Oturan, *Chem. Rev.*, **109**, 6570 (2009).

108. E. Guinea, C. Arias, P. L. Cabot, J. A. Garrido, R. M. Rodríguez, F. Centellas and E. Brillas, *Water Res.*, **42**, 499 (2008).

109. M. Zhou, Q. Yu, L. Lei and G. Barton, *Sep. Purif. Technol.*, **57**, 380 (2007).

110. C. Sáez, M. A. Rodrigo, A. S. Fajardo and C. A. Martínez-Huitle, in *Electrochemical Water and Wastewater Treatment*, p. 165–192, Butterworth-Heinemann (2018).

111. M. Hou, Y. Chu, X. Li, H. Wang, W. Yao, G. Yu, S. Murayama and Y. Wang, *J. Hazard. Mater.*, **319**, 61 (2016).

112. H. Wang, S. Yuan, J. Zhan, Y. Wang, G. Yu, S. Deng, J. Huang and B. Wang, *Water Res.*, **80**, 20 (2015).

113. Y. Zhang, X. Xu, J. Cai, Y. Pan and M. Zhou, *Chemosphere*, 266, 129063 (2021).

114. Q. Zhang, M. Zhou, Z. Lang, X. Du, J. Cai and L. Han, *Chem. Eng. J.*, **413**, 127564 (2021).

115. S. C. Perry, D. Pangotra, L. Vieira, L. Csepei, V. Sieber, L. Wang, C. Ponce de León and F. C. Walsh, *Nat. Rev. Chem.*, **3**, 442 (2019).

116. A. A. Márquez, I. Sirés, E. Brillas and J. L. Nava, *Chemosphere*, **259**, 127466 (2020).

117. O. M. Cornejo, M. Ortiz, Z. G. Aguilar and J. L. Nava, *Chemosphere*, **271**, 129804 (2021).

118. F. C. Walsh and G. W. Reade, *Stud. Environ. Sci.*, **59**, 03 (1994c).

119. F. Fu and Q. Wang, *J. Environ. Manage.*, **92**, 407 (2011).

120. S. Kumar, P. K. Sahoo and A. K. Satpati, *Electrochim. Acta*, **333**, 135467 (2020).

121. H. A. Maitlo, J. H. Kim, K. Kim, J. Y. Park and A. Khan, *J. Clean. Prod.*, **207**, 67 (2019).

122. A. Sari, D. Çitak and M. Tuzen, *Chem. Eng. J.*, **162**, 521 (2010).

123. S. Wadhawan, A. Jain, J. Nayyar and S. K. Mehta, *J. Water Process Eng.*, **33**, 101038 (2020).

124. L. Luo, X. Shen, L. Song, Y. Zhang, B. Zhu, J. Liu, Q. Chen, Z. Chen and L. Zhang, J. *Alloys Compd.*, **779**, 599 (2019).

125. A. Afkhami, T. Madrakian, A. Amini and Z. Karimi, *J. Hazard. Mater.*, **150**, 408 (2008).

126. F. M. Allioux, P. Kapruwan, N. Milne, L. Kong, J. Fattaccioli, Y. Chen and L. F. Dumée, *Sep. Purif. Technol.*, **194**, 26 (2018).

127. B. M. Babić, S. K. Milonjić, M. J. Polovina, S. Čupić and B. V. Kaludjerović, *Carbon*, **40**, 1109 (2002).

128. C. Faur-Brasquet, K. Kadirvelu and P. Le Cloirec, *Carbon*, **40**, 2387 (2002).

129. L. L. Matović, N. S. Vukelić, U. D. Jovanović, K. R. Kumrić, J. B. Krstić, B. M. Babić and A. B. Dukić, *Arab. J. Chem.*, **12**, 4446 (2019).

130. D. Yaniv and M. Ariel, *J. Electroanal. Chem. Interf. Electrochem.*, **79**, 159 (1977).

131. C. Kim, P. Srimuk, J. Lee, S. Fleischmann, M. Aslan and V. Presser, *Carbon*, **122**, 329 (2017).

132. T. Wu, G. Wang, F. Zhan, Q. Dong, Q. Ren, J. Wang and J. Qiu, *Water Res.*, **93**, 30 (2016).

133. J. Lee, S. Seo, S. Yun and S. Moon, *Water Res.*, **45**, 5375 (2011).

134. M. A. Luciano, H. Ribeiro, G. E. Bruch and G. G. Silva, *J. Electroanal. Chem.*, **859**, 113840 (2020).

135. M. E. Suss, S. Porada, X. Sun, P. M. Biesheuvel, J. Yoon and V. Presser, *Energy Environ. Sci.*, **8**, 2296 (2015).

136. A. Thamilselvan, K. Govindan, A. S. Nesaraj, S. U. Maheswari, Y. Oren, M. Noel and E. J. James, *Electrochim. Acta*, **279**, 24 (2018).

137. X. Liu and J. Wang, *Sci. Total Environ.*, **749**, 141524 (2020).

138. X. Chen, D. Chen, N. Li, Q. Xu, H. Li, J. He and J. Lu, *J. Membr. Sci.*, **567**, 209 (2018).

139. J. M. Gonzalez, L. R. Murphy, C. J. Penn, V. M. Boddu and L. L. Sanders, *Int. Soil Water Conse. Res.*, **8**, 205 (2020).

140. B. Jaleh, S. Karami, M. Sajjadi, B. Feizi, S. Azizian, M. Nasrollahzadeh and R. S. Varma, *Chemosphere*, **246**, 125755 (2020).

141. M. T. Z. Myint and J. Dutta, *Desalination*, **305**, 24 (2012)

142. H. H. Kyaw, M. T. Myint, S. Al-Harthi and M. Al-Abri, *J. Hazard. Mater.*, **385**, 121565 (2020).

143. S. W. Kim, D. H. Seo, X. Ma, G. Ceder and K. Kang, *Adv. Energy Mater.*, **2**, 710 (2012).

144. R. D. Mckerracher, A. Holland, A. Cruden and R. G. Wills, *Carbon*, **144**, 333 (2019).

145. V. Verma, S. Kumar, W. Manalastas, R. Satish, M. Srinivasan, *Adv. Sustain. Syst.*, **3**, 1800111 (2019).

146. N. Loeffler, D. Bresser, S. Passerini and M. Copley, *Johnson Matthey Technol. Rev.*, **59**, 34 (2015).

147. Z. Ogumi and M. Inaba, *Bull. Chem. Soc. Jpn.*, **71**, 521 (1998).

148. P. Zhang, C. Peng, X. Liu, F. Dong, H. Xu, J. Yang and S. Zheng, *ACS Appl. Mater. Interfaces*, **11**, 44325 (2019).

149. I. Isaev, G. Salitra, A. Soffer, Y. S. Cohen, D. Aurbach and J. Fischer, *J. Power Sources*, **119**, 28 (2003).

150. E. Ventosa, W. Xia, S. Klink, F. La Mantia, M. Muhler and W. Schuhmann, *Electrochim. Acta*, **65**, 22 (2012).

151. N. Imanishi, H. Kashiwagi, T. Ichikawa, Y. Takeda and O. Yamamoto, *J. Electrochem. Soc.*, **140**, 315 (1993).

152. M. B. Pinson and M. Z. Bazant, *J. Electrochem. Soc.*, **160**, A243 (2013).

153. Y. Liu, X. Fang, M. Ge, J. Rong, C. Shen, A. Zhang, H. A. Enaya and C. Zhou, *Nano Energy*, **16**, 399 (2015).

154. L. Y. Yang, H. Z. Li, L. Z. Cheng, S. T. Li, J. Liu, J. Min, K. J. Zhu, H. Wang and M. Lei, *J. Alloys and Compd.*, **726**, 837 (2017).

155. M. Balogun, W. Qiu, F. Lyu, Y. Luo, H. Meng, J. Li, W. Mai, L. Mai and Y. Tong, Nano *Energy*, **26**, 446 (2016).

156. Y. Fu, J. Hu, Q. Wang, D. Lin, K. Li and L. Zhou, *Carbon*, **150**, 76 (2019).

157. Q. Liu, L. Wang, X. Liu, P. Yu, C. Tian and H. Fu, *Sci. China Mater.*, **62**, 624 (2019).

158. L. Wang, D. Shao, J. Guo, S. Zhang and Y. Lu, *Energy Technol.*, **8**, 1901003 (2020).

159. M. Tamilselvan, T. V. Sreekanth, K. Yoo and J. Kim, *Appl. Surf. Sci.*, **529**, 147077 (2020).

160. J. Zhang, W. Wang, R. Shi, W. Wang, S. Wang, F. Kang and B. Li, *Carbon*, **155**, 50 (2019).

161. A. Wang, W. Zhou, A. Huang, M. Chen, J. Chen, Q. Tian and J. Xu, *J. Colloid Interface Sci.*, **577**, 256 (2020).

162. J. Yin, Z. Li, Y. Yu, Y. Lv, K. Song, B. Yang, L. Yuan and X. Hu, *Ceram. Int.*, **45**, 13401 (2019).

163. J. Li, Y. Deng, L. Leng, K. Sun, L. Huang, H. Song and S. Liao, *ACS Sustain. Chem. Eng.*, **7**, 2296 (2019).

164. K. Shen, S. Cai, R. Ling, J. Guo, D. Xie, J. Sun, J. Wei and X. Sun, *J. Alloys Compd.*, **835**, 155156 (2020).

165. M. Rychcik and M. Skyllas-Kazacos, *J. Power Sources*, **19**, 45 (1987).

166. A. Forner-Cuenca and F. R. Brushett, *Curr. Opin. Electrochem.*, **18**, 113 (2019).

167. O. C. Esan, X. Shi, Z. Pan, X. Huo, L. An and T. S. Zhao, *Adv. Energy Mater.*, **10**, 2000758 (2020).

168. A. Forner-Cuenca, E. E. Penn, A. M. Oliveira and F. R. Brushett, *J. Electrochem. Soc.*, **166**, A2230 (2019).

169. J. Zhu, L. Kong, X. Shen, G. Zhu, Z. Ji, K. Xu, H. Zhou, X. Yue and B. Li, *J. Electroanal. Chem.*, **873**, 114390 (2020).

170. N. Choudhary, C. Li, J. Moore, N. Nagaiah, L. Zhai, Y. Jung and J. Thomas, *Adv. Mater.*, **29**, 1605336 (2017).

171. P. Yu, Y. Li, X. Zhao, L. Wu and Q. Zhang, *Langmuir*, **30**, 5306 (2014).

172. M. Hashemi, M. S. Rahmanifar, M. F. El-Kady, A. Noori, M. F. Mousavi and R. B. Kaner, *Nano Energy*, **44**, 489 (2018).

173. J. Liu, Q. Wang and P. Liu, *Colloids Surf. A*, **588**, 124388 (2020).

174. X. Liang, K. Chen D. Xue, *Adv. Energy Mater.*, **8**, 1703329 (2018).

175. C. Zhou, J. Wang, X. Yan, X. Yuan, D. Wang, Y. Zhu and X. Cheng, *Ceram. Int.*, **45**, 21534 (2019).

176. S. Asim, M. S. Javed, S. Hussain, M. Rana, F. Iram, D. Lv, M. Hashim, M. Saleem, M. Khalid, R. Jawaria, Z. Ullah and N. Gull, *Electrochim. Acta*, **326**, 135009 (2019).

177. Y. Zhang, Z. Hu, Y. An, B. Guo, N. An, Y. Liang and H. Wu, *J. Power Sources*, **311**, 121 (2016).

178. Z. Tabti, R. Ruiz-Rosas, C. Quijada, D. Cazorla-Amorós and E. Morallón, *ACS Appl. Mater. Interfaces*, **6**, 11682 (2014).

179. A. Mishra, N. P. Shetti, S. Basu, K. R. Reddy and T. M. Aminabhavi, *ChemElectroChem*, **6**, 5771 (2019).

180. M. M. Ovhal, N. Kumar, S. K. Hong, H. W. Lee and J. W. Kang, *J. Alloys Compd.*, **828**, 154447 (2020).

181. L. Xing, X. Liu, T. Alaje, R. Kumar, M. Mamlouk and K. Scott, *Energy*, **73**, 618 (2014).

182. E. Carcadea, M. Varlam, M. Ismail, D. B. Ingham, A. Marinoiu, M. Raceanu, C. Jianu, L. Patularu and D. Ion-Ebrasu, *Int. J. Hydrog. Energy*, **45**, 7968 (2020).

183. Y. Wang, C. Y. Wang and K. S. Chen, *Electrochim. Acta*, **52**, 3965 (2007).

184. Y. Gao, T. Jin and X. Wu, *Energies*, **13**, 572 (2020).

185. S. Huo, J. W. Park, P. He, D. Wang and K. Jiao, *Int. J. Heat Mass Transf.*, **112**, 891 (2017).

186. K. A. Nagy, I. Y. Tóth, G. Ballai, A. T. Varga, I. Szenti, D. Sebők, J. Kopniczky, B. Hopp and A. Kukovecz, *J. Mol. Liq.*, **304**, 112698 (2020).

187. V. M. Truong, C. L. Wang, M. Yang and H. Yang, *J. Power Sources*, **402**, 301 (2018).

188. B. Fu, T. Xu, X. Guo, P. Liang, X. Huang and X. Zhang, *J. Clean. Prod.*, **229**, 542 (2019).

189. J.C. Lee, T. Shay and S.K. Chang, *J. Fuel Cell Sci. Tech.*, **8**, 031007-1 (2011).

190. A. P. Manso, F. F. Marzo, J. Barranco, X. Garikano and M. G. Mujika, *Int. J. Hydrog. Energy*, **37**, 15256 (2012).

191. M. H. Osman, A. A. Shah and F. C. Walsh, *Biosens. Bioelectron.*, **26**, 953 (2010).

192. B. Yu, L. Feng, Y. He, L. Yang and Y. Xun, *J. Hazard. Mater.*, **401**, 123394 (2021).

193. Y. Chen, L. Chen, P. Li, Y. Xu, M. Fan, S. Zhu and S. Shen, *Energy*, **109**, 620 (2016).

194. M. Wang, Z. Wang, F. Hu, L. Fan X. Zhang, *Carbon Resour. Convers.*, **3**, 76 (2020).

195. M. Tavakolian, H. G. Taleghani and M. Khorshidian, *Int. J. Hydrog. Energy*, **45**, 23533 (2020).

196. E. Blanchet, B. Erable, M. L. De Solan and A. Bergel, *Electrochem. Commun.*, **66**, 38 (2016).

197. J. Zhang, J. Li, D. Ye, X. Zhu, Q. Liao and B. Zhang, *Int. J. Hydrog. Energy*, **39**, 19148 (2014).

198. J. Liu, Junfeng Liu, W. He, Y. Qu, N. Ren and Y. Feng, *J. Power Sources*, **265**, 391 (2014).

199. J. Lai, S. Li, F. Wu, M. Saqib, R. Luque and G. Xu, *Energy Environ. Sci.*, **9**, 1210 (2016). M. Fan, H. Chen, Y. Wu, L. L. Feng, Y. Liu, G. D. Li and X. Zou, *J. Mater. Chem. A*, **3**, 16320 (2015).

200. J. González-García, P. Bonete, E. Expósito, V. Montiel, A. Aldaz and R. Torregrosa-Maciá, *J. Mater. Chem.*, 9, **419** (1999)

Table 1. Carbon cloth types and structural properties.

CC name	Weave type	Filament count	Thickness / mm	Weight per unit area / g m^{-2}	Precursor
CF-PW-210-100[a]	1×1 Plain	3k	0.3	210	Rayon
CF-PL-90-015[b]	1×1 Plain	1k	0.1	90	-
HF84[c]	Plain	1k	0.14	84	PAN
HF130[c]	Plain	1k	0.17	127	PAN
HF162[c]	Plain	3k	0.22	162	PAN
CF-22-210-125[a]	2×2 Twill	3k	0.28	210	Rayon
CF-22-240-125[a]	2×2 Twill	3k	0.32	240	Rayon
CF-22-416-125[a]	2×2 Twill	12k	0.45	416	Rayon
CF-22-450-125[a]	2×2 Twill	12k	0.65	450	Rayon
CF-22-650-125[a]	2×2 Twill	12k	0.9	650	Rayon
HF286[c]	4-harness Satin	3k	0.25	197	PAN
SGP-203-CS[c]	4-harness Satin	6k	0.27	203	PAN
CF-5HS-375-1250[a]	5-harness Satin	6k	0.53	375	PAN
PX35-SW48-50[d]	5-harness Satin	50k	2.38	1640	PAN
AGP-370-8H[c]	8-harness Satin	3k	0.35	375	PAN
PX30-KF07[d]	Single knit	-	1	250	PAN
ACF-KF-130[e]	Knitted	-	0.4	130	Pitch

[a]Mitsubishi Rayon Co. Ltd., [b]Toray Industries Inc., [c]Hexcel®, [d]Zoltek Corp., [e]Flips India Engineering©, - Not reported

Table 2. In-plane and through-plane properties for carbonaceous electrodes based on fibres.

Electrode type	Permeability / m^2		Tortuosity		Electrical resistivity / Ω cm	
	In-plane	Through-plane	In-plane	Through-plane	In-plane	Through-plane
Woven						
CC – Zoltek[9]	8×10^{-10}	9×10^{-10}	-	-	-	3
CC – NHCBA[9]	9.5×10^{-10}	7.5×10^{-10}	-	-	-	1
E-Tek Cloth A[11]	5.5×10^{-10}	7×10^{-11}	-	-	-	-
CC Plain – Digital construction[183]	-	0.9×10^{-12}	1.1	1.35	-	-
CC – ELAT hydrophilic plain / 200[10]	69.4×10^{-12}*	-	1.1*	-	0.47*	-
CC – ELAT hydrophilic plain / 400[10]	69.4×10^{-12}*	-	1.1*	-	0.45*	-
Non-woven						
Carbon felt – GFD5[19]	-	-	-	-	< 0.3	< 0.5
Carbon felt – GFA5[19]	-	-	-	-	< 0.5	< 1.5
Carbon felt - Le Carbone Lorraine[196]	6.9×10^{-11}*	-	4.95*	-	0.27*	-
Carbon paper – SGL10AA / 200[31]	37.4×10^{-12}*	-	1.8*	-	0.74*	-
Carbon paper - SGL10AA / 400[31]	37.4×10^{-12}*	-	1.8*	-	0.75*	-

Data is taken under different conditions of material compression (respect to its original thickness) and porosity, a direct comparison might not be valid for all the material. Please refer to the original documents when making comparisons.

*Measurement direction not specified in document. Placed in the "In-plane" column for convenience. - Not reported

Table 3. Active materials on CC used for OER and HER.

	Electrode name	Main functional group	Bare material		Functionalised material		Mass loading (mg cm^{-2})	Electrolyte	Durability (h)	Ref
			η (V)*	Tafel slope (mV dec^{-1})	η (V)*	Tafel slope (mV dec^{-1})				
OER	OCC-8	O-	649 (5)	167	527 (10)	82	-	0.1 M KOH	6.6	77
	PAN-CCC	N-	382 (10)	118	351 (10)	88	-	1.0 M NaOH	15	78
	ONPPGC/OCC	O-, N-, P-	600 (10)	423	410 (10)	83	0.1	1.0 M KOH	5	199
	EACC-Co-1000	$Co(OH)_2$, CoO_x, Co	-	55	340 (10)	52	-	0.1 M KOH	4.2	4
	CC-Co-1000				400 (10)	87			-	
	$CuCo_3$Sz-L-Cy/CC	Cu and Co	-	-	1576 (50)	127	2	1.0 M KOH	48	80
HER	PAN-CCC	N-	300 (10)	-228	233 (10)	135	-	1.0 M NaOH	15	78
	Mo_2C/CC	Mo-micro islands	160 (10)	-128	140 (10)	124	1.5	0.5 M H_2SO_4	15	199
	CoP/CC	CoP nanowire arrays	-	-	67 (10)	51	0.92	0.5 M H_2SO_4	22.2	200
					45 (10)	93		1.0 M PBS	-	
					209 (10)	129		1.0 M KOH	-	
	ONPPGC/OCC	O-, N-, P-	636	-193	446 (10)	154	0.1	1.0 M KOH	5	199
	EACC-Co-500	$Co(2p_{1/2}$-$2p_{3/2})$	-	-168	195 (10)	142	-	0.1 M KOH	4.2	4
	ReX_2@PCC	$ReSe_2$ nanoflakes	-	-	140 (10)	64	-	0.5 M H_2SO_4	11.1	79

* η ( ) number inside parenthesis refers to current density achieved with the indicated overpotential. (5), (10) and (50) for 5, 10 and 50 mA cm^{-2}, respectively. PBS - Phosphate-buffered saline. - Data not reported.

Figure Captions

Figure 1. CC timeline. A. Introduction of carbonaceous materials, B. Fundamental studies and applications of CC electrodes.

Figure 2. A. Carbon fibre production stages, B. Carbon cloth manufacturing process, C. Cloth weaving and knitting patterns, D. Weave cloth structure main relations.

Figure 3. Carbon cloth structure. A. Multimodal scale pores, B. CC anisotropic transport paths.

Figure 4. Electrochemical reactors utilising CC electrodes. A. Conventional three-electrode cell,[47] B. Benthic microbial fuel cell, C. Electrosorption cell,[50] D. Filter-press type electrolyser,[51] E. Spiral wound microbial fuel cell,[52] F. Commercial redox flow battery scheme.[54] With permission of Elsevier.[47,51-52,54] Copyright IWA Publishing 2018.[50]

Figure 5. *F-curves* for residence time distributions in two different energy conversion devices. A. Compact spiral wound microbial fuel cell on single ACC sheet (SW-1), B. Compact spiral wound microbial fuel cell on two ACC sheets (SW-2).[52] C. Interdigitated redox flow battery with 0.03 L min^{-1} flow rate, D. Interdigitated redox flow battery with a volumetric flow rate of 0.04 L min^{-1}.[54] Reproduced with permission of Elsevier.

Figure 6. A. Pressure drop comparison in a redox flow battery equipped with CC and carbon paper electrodes.[10] B, Dimensionless concentration decay for pyridine, phenol and NSA adsorption on ACC.[66] C. Potential drop *vs* current (apparent global resistance slope) for CC-

3257 of different lengths (38, 20, 10.5 cm), D. Potential drop *vs* current (apparent global resistance slope) for CC-3872.[56] Reproduced with permission from Elsevier,[10,66] and Springer.[56]

Figure 7. A. Dimensionless cumulative function, F(t), for different flow rates. Experimental RTD data (dots) are predicted by CFD (solid line). B. Velocity field within the CC electrode; the insets (I) and (II) represent near inflow and outflow zones on arrow velocity surface. C. Velocity profile within the CC electrode at different flow rates (over the cutting line (III)) Data taken from G. Aparicio Mauricio *et al.*[54] with permission from Elsevier.

Figure 8. Controlled potential electrolysis of Cu^{2+} ion. Decay of current through graphite cloth electrode (dotted line) and copper ion removal percentages (continuous line), both as a function of the electrolysis time (Cathode potential: -0.7 V *vs* SCE).[129] Reproduced with permission of Elsevier.

Figure 9. Specific capacity *vs* specific discharge current (respect to the mass of catalyst material) for different types of battery and electrode substrate. CC, G (graphite electrode), CF (carbon felt), CNT (carbon nanotubes) and CPw (carbon powder).

Figure 10. 3D porous electrodes reconstructed from computational X-ray tomography. Non-woven structure: a) Freudenberg paper, b) SGL paper, and woven structure: c) CC.[70] Reproduced with permission of Elsevier.

Figure 11. Power and current density for different CC anodes in MFCs. Comparison of performance in bare CC (open figure) and modified CC (filled figure). (⬣) Electrochemical oxidation and chemical treatment,[197] (⬟) Chemical treatment,[197] (◀) Composite (GAC/CC) in flow-through mode,[187] (▼) Composite (GAC/CC) in static mode,[187] (■) Electrochemical oxidation,[198] (●) Metal oxide and polymer insertion,[193] (▲) Chemical treatment,[193] (◆) Polymer insertion.[48]

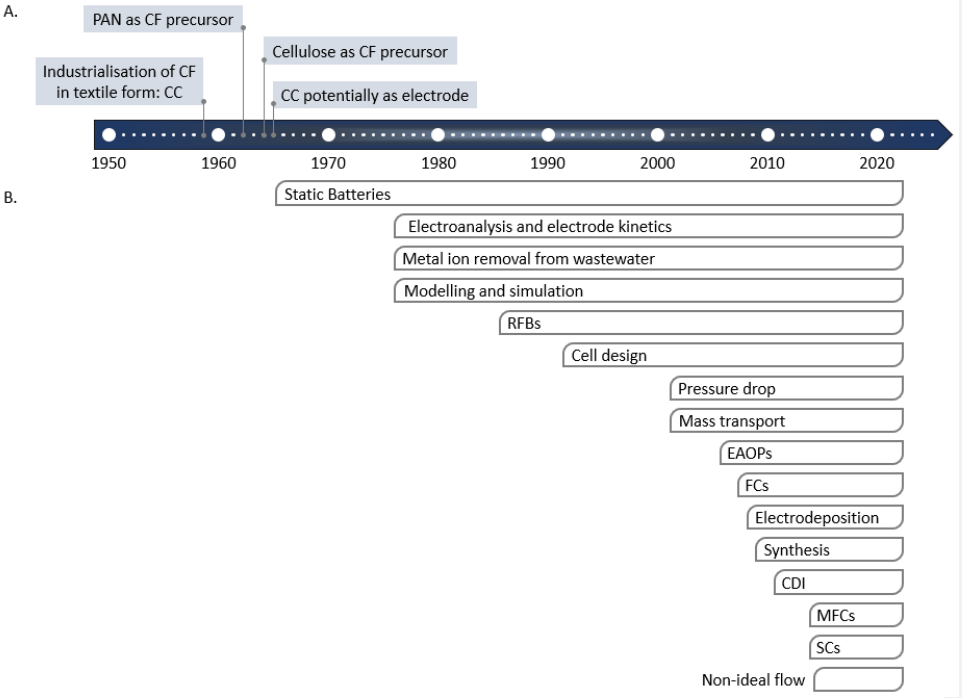
A.
PAN as CF precursor
Cellulose as CF precursor
Industrialisation of CF in textile form: CC
CC potentially as electrode
1950
1960
1970
1980
1990
2000
2010
2020
B.
Static Batteries
Electroanalysis and electrode kinetics
Metal ion removal from wastewater
Modelling and simulation
RFBs
Cell design
Pressure drop
Mass transport
EAOPs
FCs
Electrodeposition
Synthesis
CDI
MFCs
SCs
Non-ideal flow

Figure 1

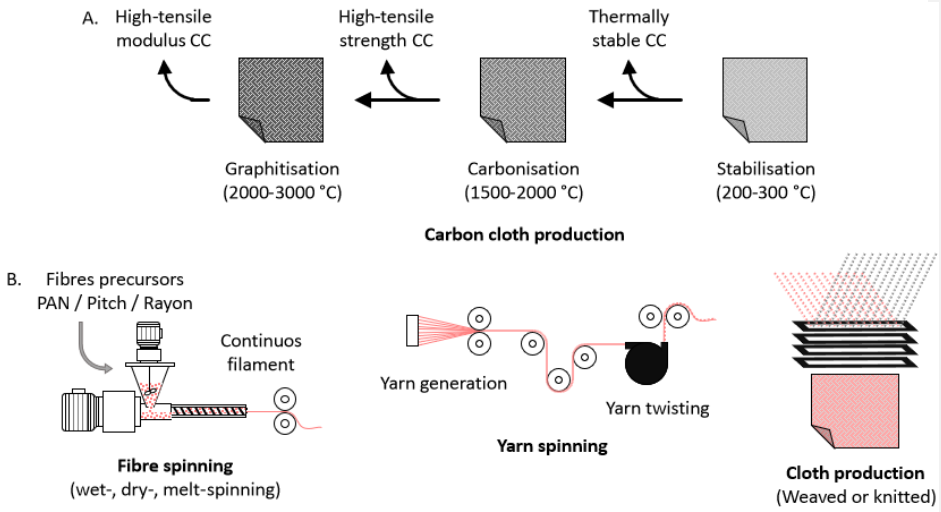

Figure 2

Commented [F C1]: 'woven' instead of 'weaved'

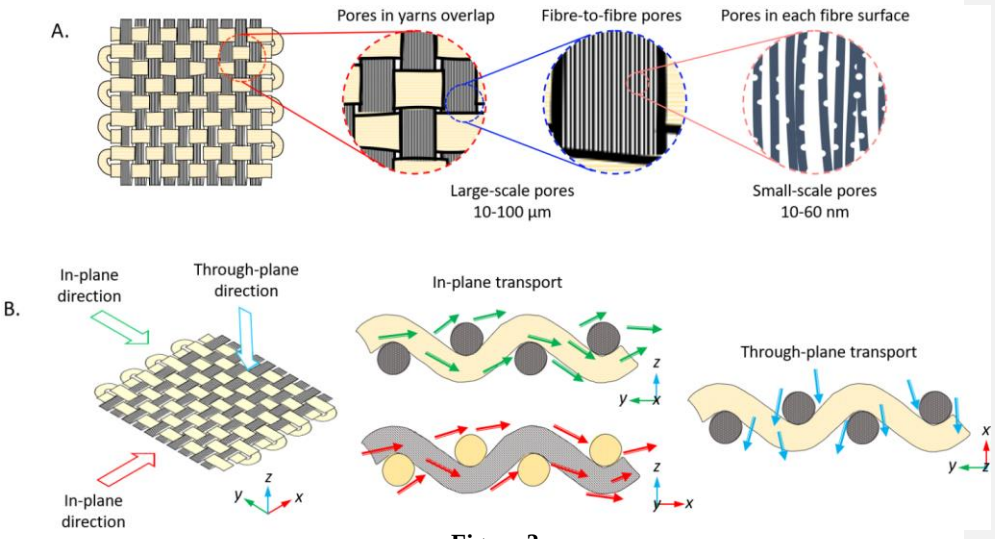
A.
Pores in yarns overlap
Fibre-to-fibre pores
Pores in each fibre surface
Large-scale pores
10-100 µm
Small-scale pores
10-60 nm
B.
In-plane direction
Through-plane direction
In-plane direction
In-plane transport
Through-plane transport

Figure 3

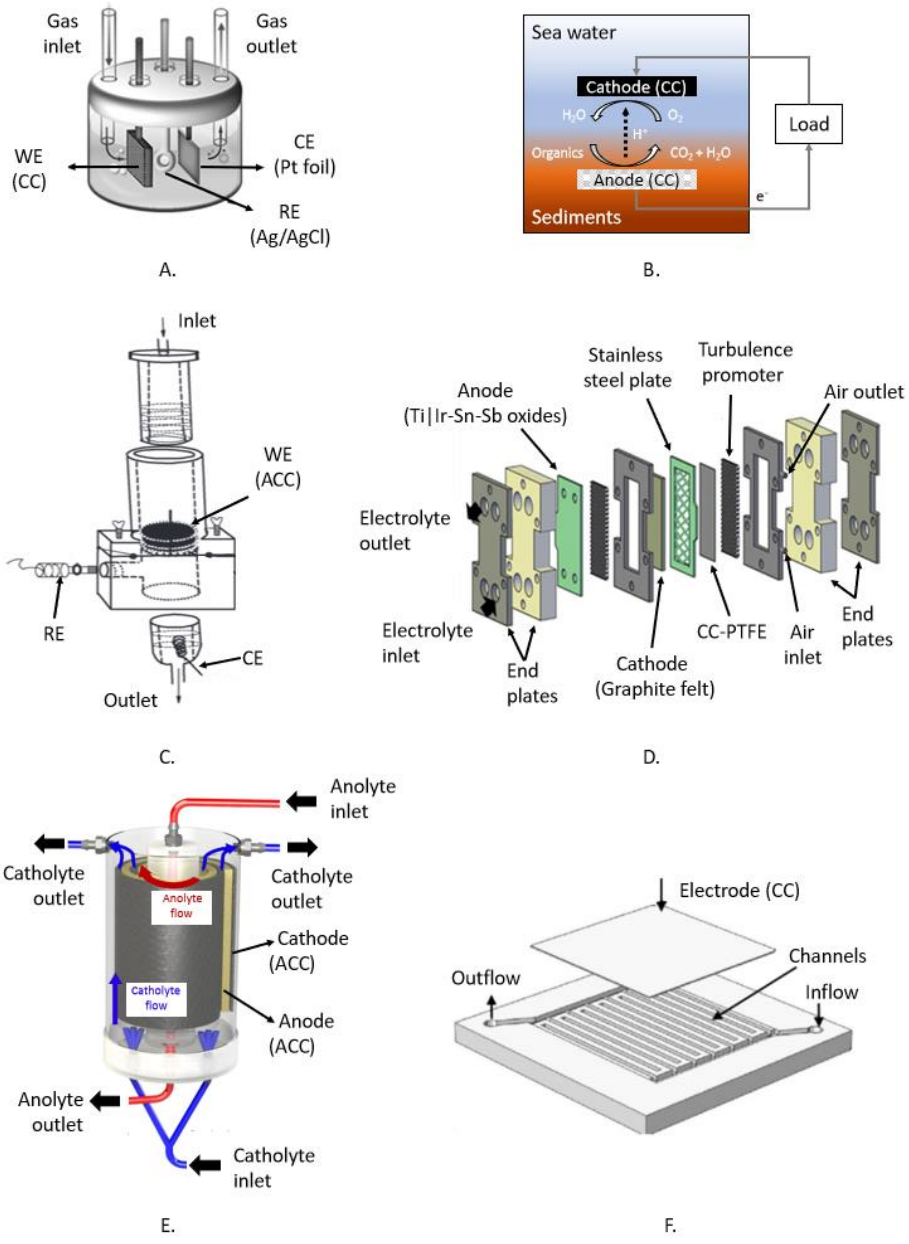
Gas inlet
Gas outlet
WE (CC)
CE (Pt foil)
RE (Ag/AgCl)
A.
Sea water
Cathode (CC)
H_2O
O_2
H^+
Organics
$CO_2 + H_2O$
Anode (CC)
Sediments
Load
e^-
B.
Inlet
WE (ACC)
RE
CE
Outlet
C.
Anode (Ti|Ir-Sn-Sb oxides)
Stainless steel plate
Turbulence promoter
Air outlet
Electrolyte outlet
Electrolyte inlet
End plates
Cathode (Graphite felt)
CC-PTFE
Air inlet
End plates
D.
Anolyte inlet
Catholyte outlet
Catholyte outlet
Anolyte flow
Cathode (ACC)
Catholyte flow
Anode (ACC)
Anolyte outlet
Catholyte inlet
E.
Electrode (CC)
Channels
Outflow
Inflow
F.

Figure 4

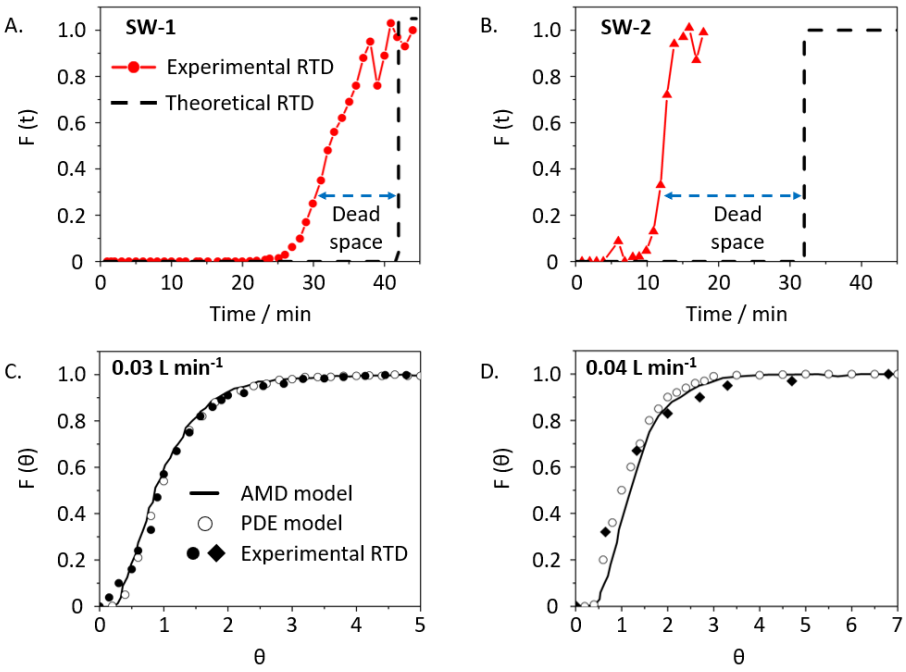
A.
SW-1
Experimental RTD
Theoretical RTD
F (t)
Dead space
Time / min
B.
SW-2
F (t)
Dead space
Time / min
C.
0.03 L min-1
AMD model
PDE model
Experimental RTD
F (θ)
θ
D.
0.04 L min-1
F (θ)
θ

Figure 5

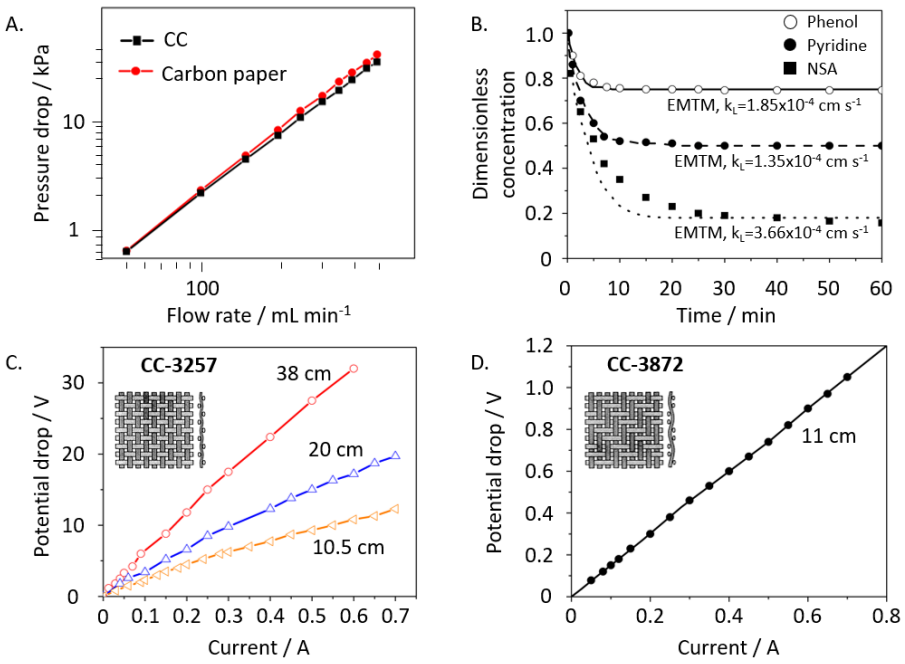
A.
CC
Carbon paper
Pressure drop / kPa
Flow rate / mL min-1
B.
Phenol
Pyridine
NSA
EMTM, kL=1.85x10-4 cm s-1
EMTM, kL=1.35x10-4 cm s-1
EMTM, kL=3.66x10-4 cm s-1
Dimensionless concentration
Time / min
C.
CC-3257
38 cm
20 cm
10.5 cm
Potential drop / V
Current / A
D.
CC-3872
11 cm
Potential drop / V
Current / A

Figure 6

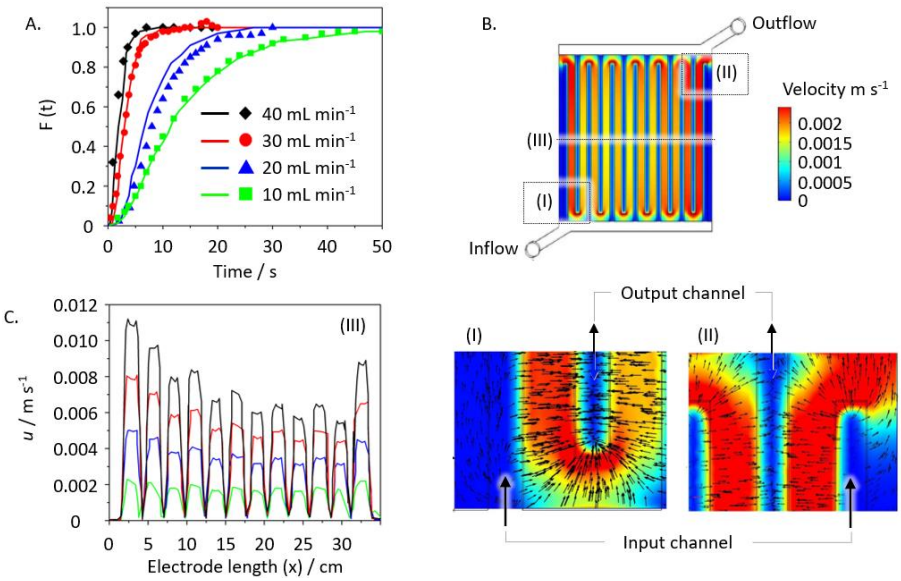
A.
F (t)
Time / s
40 mL min-1
30 mL min-1
20 mL min-1
10 mL min-1
B.
Outflow
Inflow
(I)
(II)
(III)
Velocity m s-1
0.002
0.0015
0.001
0.0005
0
C.
u / m s-1
Electrode length (x) / cm
Output channel
Input channel

Figure 7

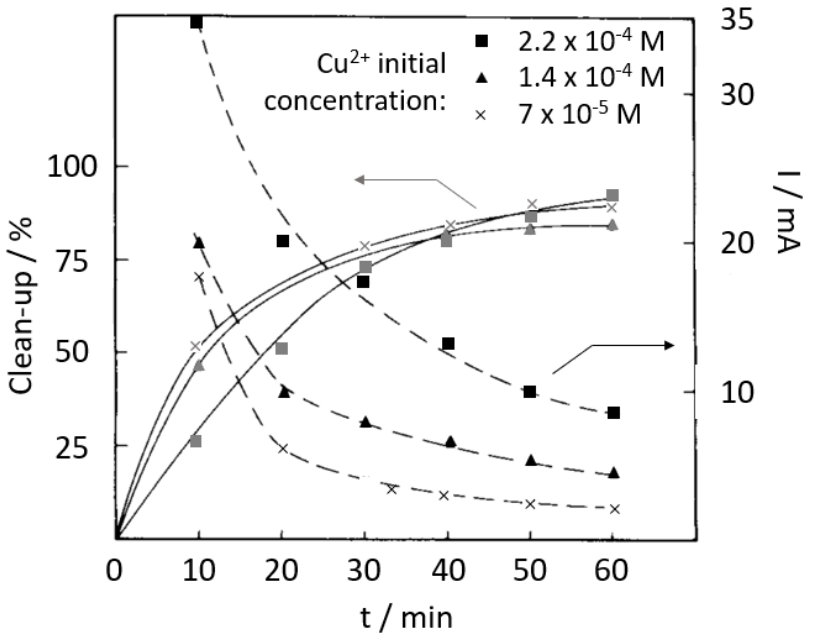
Cu2+ initial concentration:
2.2 x 10-4 M
1.4 x 10-4 M
7 x 10-5 M
Clean-up / %
I / mA
t / min
100
75
50
25
35
30
20
10
0
10
20
30
40
50
60

Figure 8

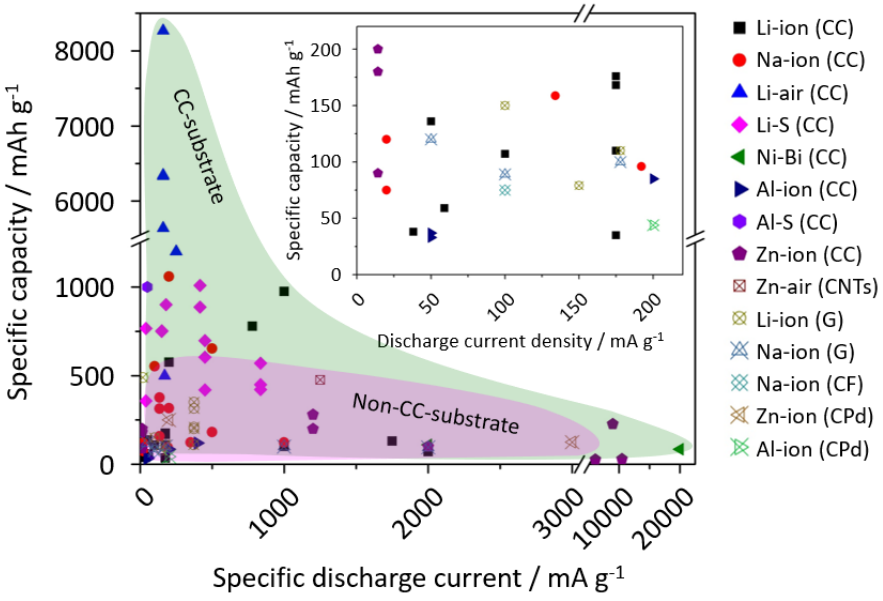
Specific capacity / mAh g-1
8000
7000
6000
1000
500
0
CC-substrate
Non-CC-substrate
Specific capacity / mAh g-1
200
150
100
50
0
0
50
100
150
200
Discharge current density / mA g-1
0
1000
2000
3000
10000
20000
Specific discharge current / mA g-1
Li-ion (CC)
Na-ion (CC)
Li-air (CC)
Li-S (CC)
Ni-Bi (CC)
Al-ion (CC)
Al-S (CC)
Zn-ion (CC)
Zn-air (CNTs)
Li-ion (G)
Na-ion (G)
Na-ion (CF)
Zn-ion (CPd)
Al-ion (CPd)

Figure 9

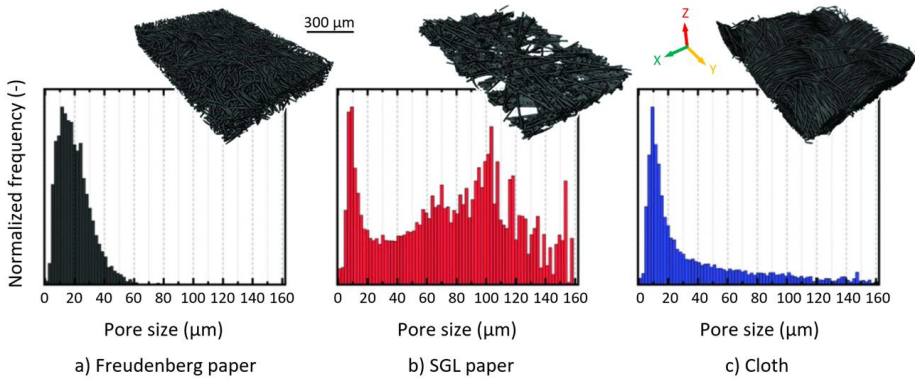
300 µm
Z
X
Y
Normalized frequency (-)
0 20 40 60 80 100 120 140 160
Pore size (µm)
a) Freudenberg paper
0 20 40 60 80 100 120 140 160
Pore size (µm)
b) SGL paper
0 20 40 60 80 100 120 140 160
Pore size (µm)
c) Cloth

Figure 10

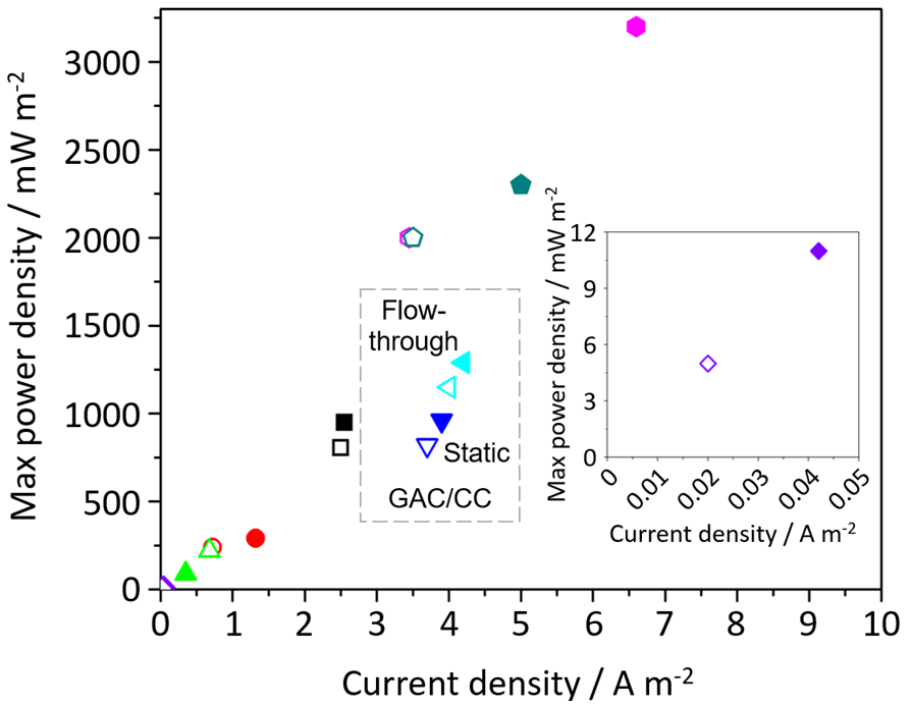
Max power density / mW m-2
Current density / A m-2
Flow-through
Static
GAC/CC
Max power density / mW m-2
Current density / A m-2

Figure 11